

## FEATURE ARTICLE

[View Article Online](#)  
[View Journal](#) | [View Issue](#)Cite this: *Chem. Commun.*, 2023, 59, 7321

## From sandwich complexes to dendrimers: journey toward applications to sensing, molecular electronics, materials science, and biomedicine†

Didier Astruc

This review links various areas of inorganic chemistry around the themes developed by our research group during the last four decades. It is firstly based on the electronic structure of iron sandwich complexes, showing how the metal electron count dictates their reactivities, with various applications (*via* C–H activation, C–C bond formation) as reducing and oxidizing agents, redox and electrocatalysts and precursors of dendrimers and catalyst templates through bursting reactions. Various electron-transfer processes and consequences are explored, including the influence of the redox state on the acidity of robust ligands and the possibility to iterate *in situ* C–H activation and C–C bond formation to build arene-cored dendrimers. Examples of how these dendrimers are functionalized are illustrated using the cross olefin metathesis reactions, with application to the synthesis of soft nanomaterials and biomaterials. Mixed and average valence complexes give rise to remarkable subsequent organometallic reactions, including the salt influence on these reactions. The stereo-electronic aspect of these mixed valencies is pointed out in star-shaped multi-ferrocenes with a frustration effect and other multi-organoiron systems, with the perspective of understanding electron-transfer processes among dendrimer redox sites involving electrostatic effects and application to redox sensing and polymer metallocene batteries. Dendritic redox sensing is summarized for biologically relevant anions such as  $\text{ATP}^{2-}$  with supramolecular exoreceptor interactions at the dendrimer periphery in parallel with the seminal work on metallocene-derived endoreceptors by Beer's group. This aspect includes the design of the first metalodendrimers that have applications in both redox sensing and micellar catalysis with nanoparticles. These properties provide the opportunity to summarize the biomedical (mostly anticancer) applications of ferrocenes, dendrimers and dendritic ferrocenes in biomedicine (in particular the contribution from our group, but not only). Finally, the use of dendrimers as templates for catalysis is illustrated with numerous reactions including C–C bond formation, click reactions and  $\text{H}_2$  production reactions.

Received 9th March 2023,  
Accepted 2nd May 2023

DOI: 10.1039/d3cc01175e

[rsc.li/chemcomm](http://rsc.li/chemcomm)

### I. Introduction

Shortly following Pauson's report 70 years ago of ferrocene with an erroneous 10-electron electronic structure<sup>1</sup> violating the century-old Langmuir's 18-electron rule,<sup>2</sup> the aromatic ground for the extraordinary robustness of ferrocene was established, justifying Woodward's proposal of the ferrocene name.<sup>3</sup> The subsequent flourishing chemistry was more that of a tridimensional super-aromatic organic compound than that representative of organo-transition-metal chemistry.<sup>4</sup> The outstanding ferrocene stability, connected to its 18-electron

structure,<sup>4–6</sup> allowed formation of a rather stable cation, 17-electron ferricenium in a variety of salts, in spite of the loss of one electron from an essentially non-bonding orbital (and Fe–Cp distance only slightly increasing compared to ferrocene), whereas most organometallic compounds do not withstand such a monoelectronic oxidation, which provokes their breakdown.<sup>7</sup> The stability of late transition-metal sandwich complexes in at least two oxidation states was used at the beginning of our research to provide a variety of electron and proton transfer processes. The latter reaction type was at the origin of the discovery of starburst reactions leading to stars and dendrimers. Then, some analogies between metalodendrimers and metal nanoparticles led us to examine and exploit their supramolecular interplay with applications to sensing, molecular electronics, materials science, catalysis and biomedicine. Herein, a review of this interdisciplinary research path and its applications is proposed.

Univ. Bordeaux, ISM, UMR CNRS No. 5255, 351 Cours de la Libération,  
33405 Talence Cedex, France. E-mail: didier.astruc@u-bordeaux.fr

† This article is dedicated to my distinguished friend and colleague Professor Henri Bouas-Laurent on the occasion of his 90th birthday.

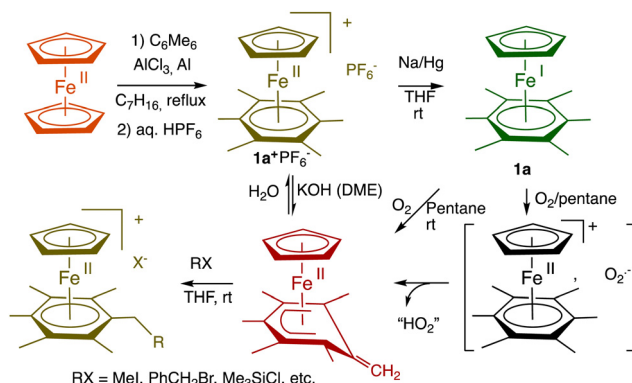


## II. Applications of the 17 and 19-electron late transition-metal sandwich complexes as reservoirs of electron holes and electrons

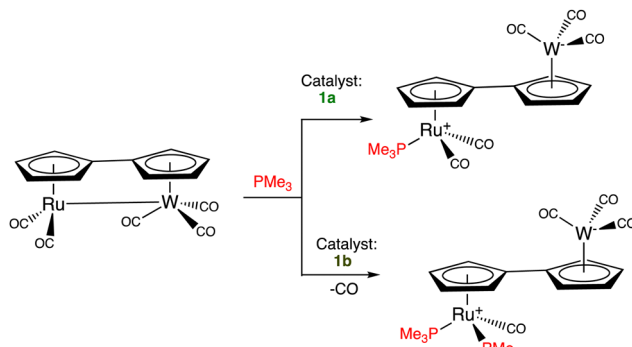
There is a rare truly organometallic reaction of ferrocene that deserved interest, namely its Lewis-acid induced cyclopentadienyl substitution by arenes upon mild heating leading to cationic arene complexes  $[\text{FeCp}(\eta^6\text{-arene})]^+\text{X}^-$  with  $\text{Cp} = \eta^5\text{-C}_5\text{H}_5$ ,  $\text{X}^- = \text{PF}_6^-$ , in which the robust 18-electron sandwich  $\text{Fe}(\text{II})$  structure is preserved.<sup>8</sup> The cationic nature of these arene  $\text{Fe}(\text{II})$  complexes allowed an “Umpolung” of arene reactivity including, for instance, reversible deprotonation of the 18-electron form, which turned out to be synthetically productive (Scheme 1, bottom). The stability of their neutral 19-electron  $\text{Fe}(\text{I})$  form such as **1a** facilitated by the presence of six methyl substituents on the arene allowed its full characterization including *inter alia* X-ray crystal structure,<sup>9</sup> <sup>1</sup>H NMR (paramagnetism),<sup>9</sup> redox potentials,<sup>10</sup> EPR (rhombic distortion)<sup>11</sup> and He(*i*) photoelectron spectroscopy (extremely low value of the ionization potential).<sup>12</sup> The exceptional electron richness of this new family of transition-metal sandwich complexes that were the first characterized stable 19-electron complexes with the new stable  $\text{Fe}(\text{I})$  oxidation state in monometallic complexes yielded a variety of electron-transfer reactions starting from that with  $\text{O}_2$  upon short contact with air (Scheme 1).<sup>12,13</sup>

Among other remarkable electron-transfer reactions of **1a** and of the analogue  $[\text{FeCp}^*(\eta^6\text{-C}_6\text{Me}_6)]$ , **1b**, in which  $\text{Cp}^* = \eta^5\text{-C}_5\text{Me}_5$ , were the single, double and triple reduction of  $\text{C}_6\text{O}_6$  depending on the reaction stoichiometry,<sup>19</sup> the generation of *N*-heterocyclic carbenes of well-known catalytic importance<sup>20</sup> and the stabilization of a new nanocomposite family by reduction of gold nanoclusters.<sup>21</sup>

Catalytic electron-transfer reactions of these  $\text{Fe}(\text{I})$  complexes of interest were the redox catalysis of nitrates and nitrites to ammonia<sup>22,23</sup> and the electron-transfer-chain (ETC) catalyzed



**Scheme 1** Synthesis and reaction with  $\text{O}_2$  of the 19-electron  $\text{Fe}(\text{I})$  complex **1a**. Due to the large difference (about 1 V) between the two redox systems  $\text{Fe}(\text{I})/\text{Fe}(\text{II})$  and  $\text{O}_2/\text{O}_2^{\bullet-}$ , electron transfer from  $\text{Fe}(\text{I})$  to  $\text{O}_2$  is very exergonic and fast, followed by deprotonation by  $\text{O}_2^{\bullet-}$  within the intermediate ion cage (from  $\text{O}_2^{\bullet-}$  EPR).<sup>14,15</sup> In THF, this cage superoxide reaction is totally inhibited by  $\text{NaPF}_6$  due to ion exchange between the two ion pairs  $[\text{Fe}(\text{II})]^+$ ,  $\text{O}_2^{\bullet-}$  and  $[\text{Na}^+, \text{PF}_6^-]$ ,<sup>16</sup> (for a review of salt effects, see ref. 17) which is reminiscent of the function of superoxide dismutase enzyme.<sup>18</sup>



**Scheme 2** ETC-catalyzed  $\text{PMe}_3$  ligand addition in the fulvalene heterobimetallic complex  $[\text{RuW}(\eta^{10},\mu^2\text{-C}_{10}\text{H}_8)(\text{CO})_5]$ . The reaction depends on the  $\text{Fe}(\text{I}/\text{II})$  redox potential of the electron-reservoir ETC catalyst (**1a** vs.  $[\text{Fe}(\eta^5\text{-C}_5\text{Me}_5)(\eta^6\text{-C}_6\text{Me}_6)]$ , **1b**). With the more electron-rich electron reservoir **1b** as ETC catalyst, two  $\text{PMe}_3$  ligands are introduced whereas, with **1a**, only one  $\text{PMe}_3$  ligand is added. ETC catalysis was pioneered by Henry Taube.<sup>27</sup>



**Didier Astruc**  
Didier Astruc born in Versailles, studied in Rennes, where he obtained two doctorate degrees with prof. René Dabard, then was a NATO post-doctoral fellow with prof. Richard R. Schrock at M. I. T., Cambridge, USA, and later spent a sabbatical year with prof. K. Peter C. Vollhardt at the University of California, Berkeley. He is professor of chemistry at the University of Bordeaux, member of the Institut Universitaire de France and of the French, German (Leopoldina) and several European Academies, and Fellow of the Royal Society of Chemistry and Chemistry Europe. His present interests are in nanomaterials and hydrogen energy.

French, German (Leopoldina) and several European Academies, and Fellow of the Royal Society of Chemistry and Chemistry Europe. His present interests are in nanomaterials and hydrogen energy.

(electrocatalytic) arene substitution in the series  $[\text{FeCp}(\text{arene})]\text{PF}_6$  by three 2-electron phosphorus donors<sup>24</sup> and CO exchange by phosphines in Vollhardt's fulvalene heterobimetallic carbonyl complexes (Scheme 2).<sup>25,26</sup>

In both types of reactions, the availability of a library of  $\text{Fe}(\text{I})$  complexes with different values of their  $\text{Fe}(\text{II})/\text{Fe}(\text{I})$  redox potential was very useful to determine the very fate of reactions. More generally, for applications in redox chemistry, a scale gathering useful transition metal sandwich complexes is represented in Fig. 1.

Finally, another useful property of the transition-metal sandwich complexes that were fully methylated on both ligands such as **1b** and decamethylmetallocenes (Co, Fe) was their ability to serve as medium-independent references in cyclic voltammetry for the determination of redox potentials.<sup>28,29</sup>



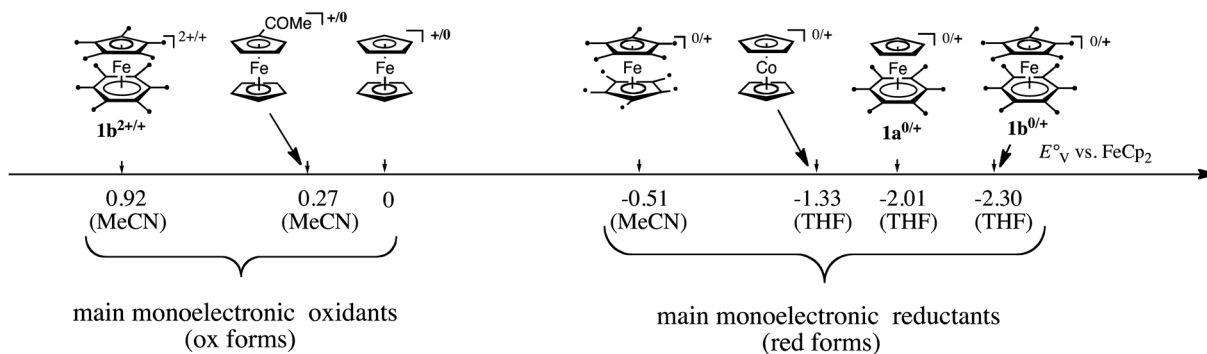
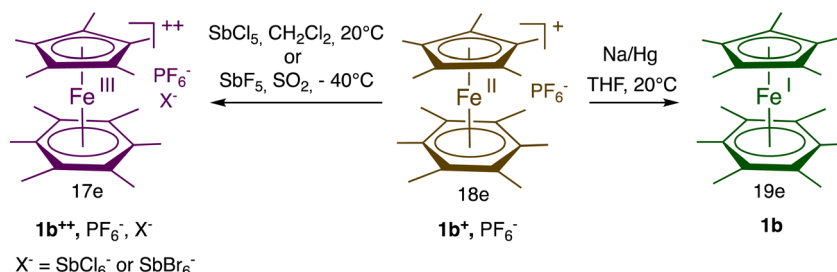


Fig. 1 Redox potential scale of useful late transition-metal sandwich complexes as redox reagents.



Scheme 3 Synthesis of the stable, fully methylated mixed sandwich Fe complexes with 17 and 19 valence electrons [ $d^5$ , Fe(III) resp.  $d^7$ , Fe(I)] that are both redox catalysts and electrocatalysts.

Indeed, the permethylated sandwich systems are more reliable than the traditional ferricinium/ferrocene redox system that is subjected to redox potential variations due to the presence of nucleophilic solvent that interact with the cationic Fe center, whereas the permethylation of the sandwich rings sterically prevents such interactions.

In ferrocene chemistry, access to the 19-electron species occurs at a cathodic potential that is too negative for applications, even if a salt of the 19-electron hexa(*t*-butyl) ferrocene anion was recently characterized at  $-30\text{ }^\circ\text{C}$ .<sup>30</sup> On the other hand, in the sandwich series  $[\text{Fe}(\eta^5\text{-C}_5\text{R}_5)(\eta^6\text{-C}_6\text{Me}_6)]^{n+}$  ( $n = 0\text{--}2$ ), the 3 oxidation states are accessible (Scheme 3)<sup>31</sup> and could be isolated with suitable counter anions for  $\mathbf{1b}^{2+}$ . Consequently, the 17-electron Fe(III) and 19-electron Fe(I) forms have been used as reservoirs of electron hole and electrons, respectively, for redox catalysis and ETC catalysis,<sup>32</sup> (electrocatalysis) (Scheme 2).<sup>27</sup>

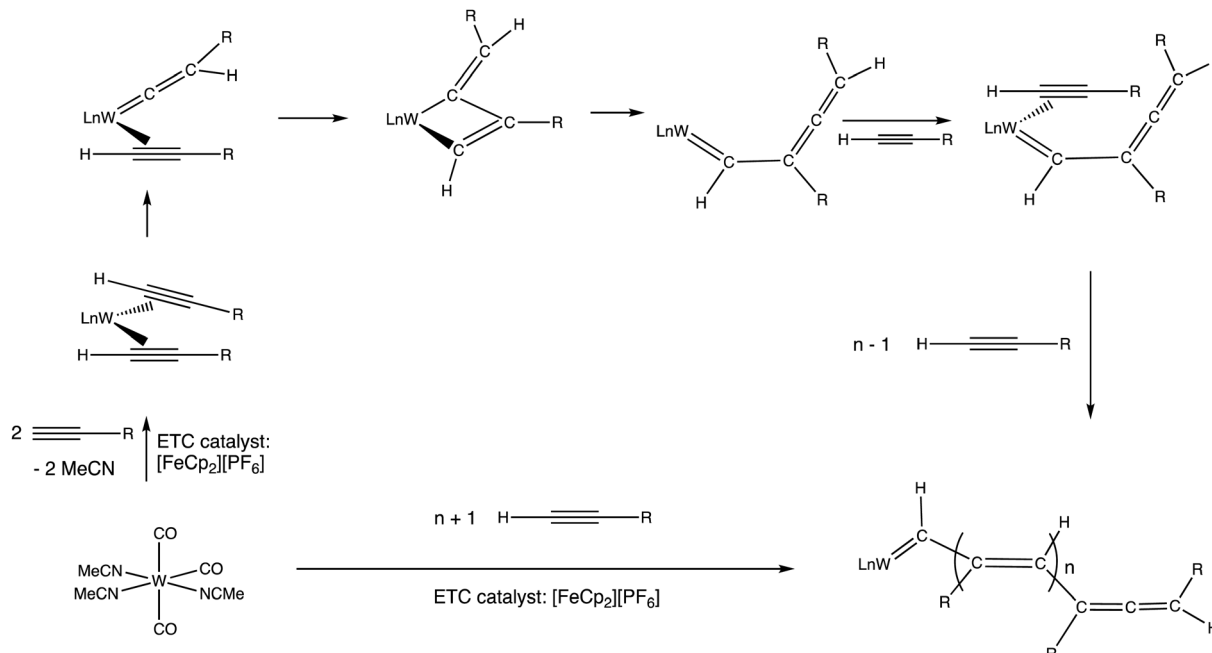
As shown early on by Wilkinson,<sup>4</sup> ferrocene is easily oxidized to ferricinium salts upon reaction with  $\text{I}_2$ ,  $\text{FeCl}_3$  or  $\text{AgNO}_3$ , and the resulting ferricinium salts are easily reduced back to ferrocene by reaction with, for instance, an acidic aqueous solution of  $\text{TiCl}_3$  or thiosulfate. The oxidizing property of ferricinium has been extensively applied to organometallic synthesis.<sup>33–35</sup> An example of catalytic redox application was shown in the combination of ferricinium with the organometallic pre-catalyst  $[\text{W}(\text{CO})_3(\text{NCMe})_3]$ , active in terminal alkyne polymerization.<sup>36,37</sup> This type of alkyne polymerization proceeds according to the Chauvin–Katz metathesis mechanism,<sup>38,39</sup> whereby the active catalyst precursor is a W-vinylidene species rearranging to a tungstacyclobutene intermediate.

The role of ferricinium therein is to accelerate, by an ETC-catalyzed reaction, the introduction of the alkyne ligand rearranging to the vinylidene ligand (Scheme 4).<sup>40</sup>

In summary, the  $\text{Fe}^1$  sandwich complexes are a rich family of electron-reservoir molecules, with a variety of substituents on the ligand rings, that undergo a variety of useful stoichiometric and catalytic electron-transfer processes in organic solvents (**1a**, **1b**, *etc.*) or in water (for instance **1c** and many others) summarized in Fig. 2. On the oxidation side, similar processes are accessible with the 17-electron ferricinium salts or, if insufficiently strong oxidant, the stronger 17-electron **1b**<sup>2+</sup> salts.

### III. From organometallic chemistry to macromolecular chemistry: the advent of dendrimers with an original bursting reaction

The dendrimer field has been pioneered in the early 1980s mostly by Tomalia with PAMAM dendrimers<sup>41</sup> and by Newkome with arborols,<sup>42</sup> and in France, the Caminade–Majoral group, in particular, has been extremely active therein.<sup>43</sup> Our story with dendrimers started when we discovered and reported in 1979 the bursting reaction of the complexes  $[\text{FeCp}(\eta^6\text{-C}_6\text{Me}_6)]\text{-}[\text{PF}_6]_9$ .<sup>9</sup> These one-pot multiple C–C branching reactions, extended to any number of methyl groups on the arene ligand, simply proceed under ambient conditions in the presence of an organic halide and a base such as *t*-BuOK or KOH in THF or



**Scheme 4** Polymerization of terminal alkyne catalyzed by a W(0) pre-catalyst according to the Chauvin–Katz metathesis mechanism. Addition of a catalytic amount of  $[\text{FeCp}_2]\text{PF}_6$  vs. the W(0) catalyst considerably accelerates the reaction (from 100 °C, hours, in the absence of  $[\text{FeCp}_2]\text{PF}_6$  to r.t. within a few minutes. Exchange of MeCN by the alkyne in the 18-electron W(0) complex is slow, but it becomes very fast at the 17-electron level. Following this exchange, the ETC cross redox step with the starting pre-catalyst is also fast due to its exergonicity, because the alkyne is a  $\pi$ -acceptor, contrary to MeCN.<sup>36</sup>

DME, respectively. Deprotonation by the base proceeds first; then, nucleophilic substitution of the halide group occurs in the organic halide by the nucleophilic benzylic carbon that was previously deprotonated. Generally, for arenes bearing methyl substituents that do not have neighbors such as in mesitylene, this deprotonation–nucleophilic reaction sequence proceeds three times on each benzylic carbon,<sup>44</sup> but it does so only twice for methyl groups that have only one methyl neighbor such as in *o*-xylene or durene,<sup>45</sup> and only once (at least for short reaction times) for methyl groups that have two methyl neighbors such as in hexamethylbenzene.<sup>46,47</sup> Organic halides that undergo such reactions include methyl iodide, benzyl bromide (including *para*-substituted derivatives) and allyl bromide. Polyallyl branching was very favorable for further functionalization of the terminal C=C bond, and the 12-electron  $\text{CpFe}^+$  could be recycled upon visible-light photolysis in the presence of mesitylene (Scheme 5).

The nona-allyl structure served as core for dendrimer construction upon three-fold multiplication of the dendrimer branches at each generation.<sup>48</sup> For this purpose, a triallylated phenol dendron was synthesized using the same  $\text{CpFe}^+$ -induced triallylation strategy.<sup>49</sup> For the divergent dendrimer growth, the construction using such a  $1 \rightarrow 3$  branching, first initiated by Newkome with arborols,<sup>50</sup> allows reaching much faster a high number of dendrimer tethers than the classic dendrimer double-branching construction. The dendrimer syntheses were followed by  $^1\text{H}$ ,  $^{13}\text{C}$  and  $^{29}\text{Si}$  NMR indicating that they were clean on the NMR accuracy till the 9th generation (theoretical number of 177 407 terminal branches), which was confirmed by monodispersity

measured by SEC (PDI = 1.00 or 1.01). The globular shape observed by HRTEM for the 9th-generation dendrimer was 16.7 nm. In AFM, a linear size progression of the layer thickness on graphitic HOPG support was observed till the 5th generation with a size of 10 nm, but from the 6th to the 9th generation, the thickness grew faster, reaching 25 nm, which presumably corresponded to a double dendrimer layer (Scheme 6 and Fig. 3).

Defects, that are inherent to the divergent dendrimer construction, were characterized in the MALDI TOF mass spectrum of the 81-allyl dendrimer; although the molecular peak was largely dominant, a small peak was observed corresponding to the lack of one dendron. The characterization data show that the total number of branches is superior to  $10^5$  at the 9th generation level. Although de Gennes predicted that PAMAM dendrimer construction was limited due to steric limit at the dendrimer periphery,<sup>51</sup> we believe that, on the contrary, our construction was not limited by the periphery bulk, because the lack of hydrogen bond at the termini allowed terminal branches to backfold toward the dendrimer core to avoid the bulky periphery. In this way, the construction is only limited by the overall dendrimer volume.

Activation of exo-cyclic C–H groups of arene ligands in the complexes  $[\text{FeCp}(\text{arene})]\text{PF}_6^-$  was useful to build more complex structures such as cyclophane, showing examples of the synthetic power of this activation type.<sup>52</sup> Since this family of complexes are directly synthesized by reaction of ferrocene with the arene, this illustrates once more the synthetic potential of ferrocene.<sup>53</sup> The  $\text{CpFe}^+$  activating group is not the only one able to activate the exocyclic C–H bonds in proton reservoir



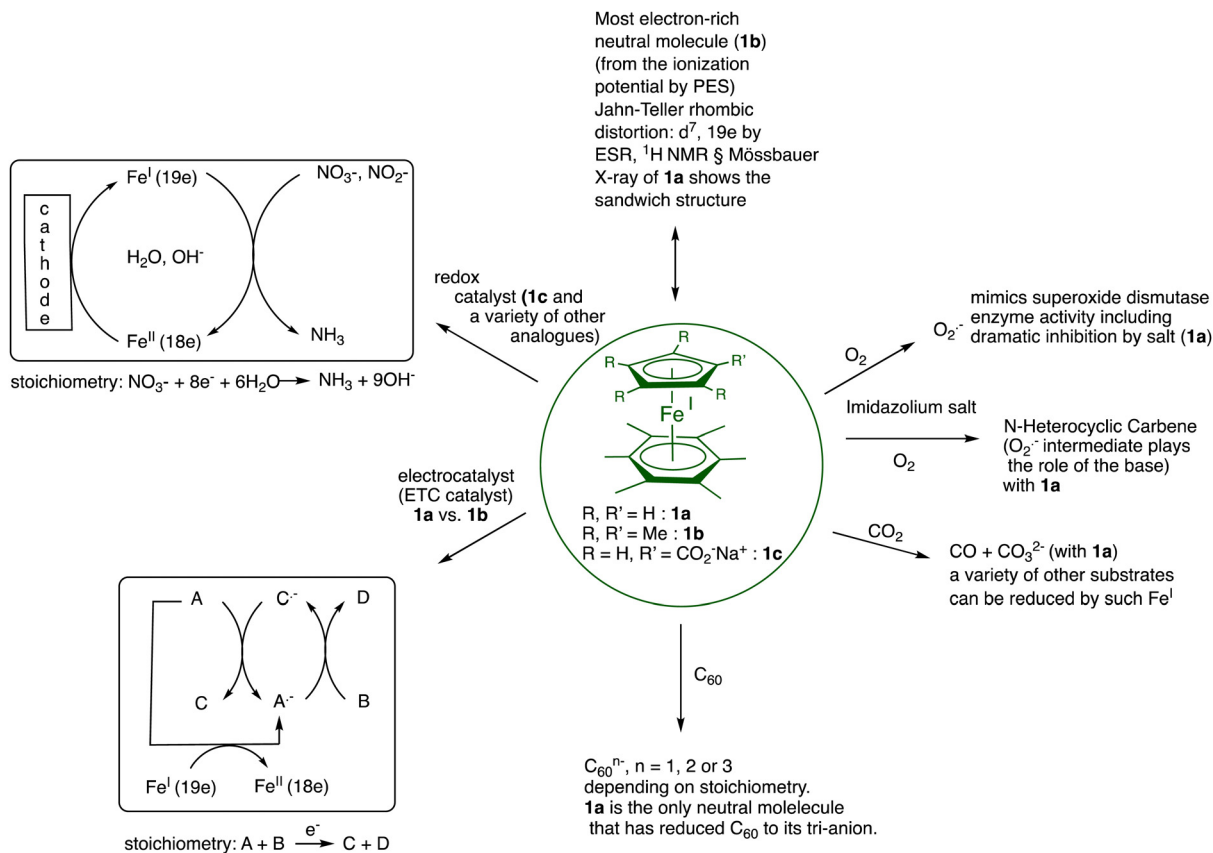
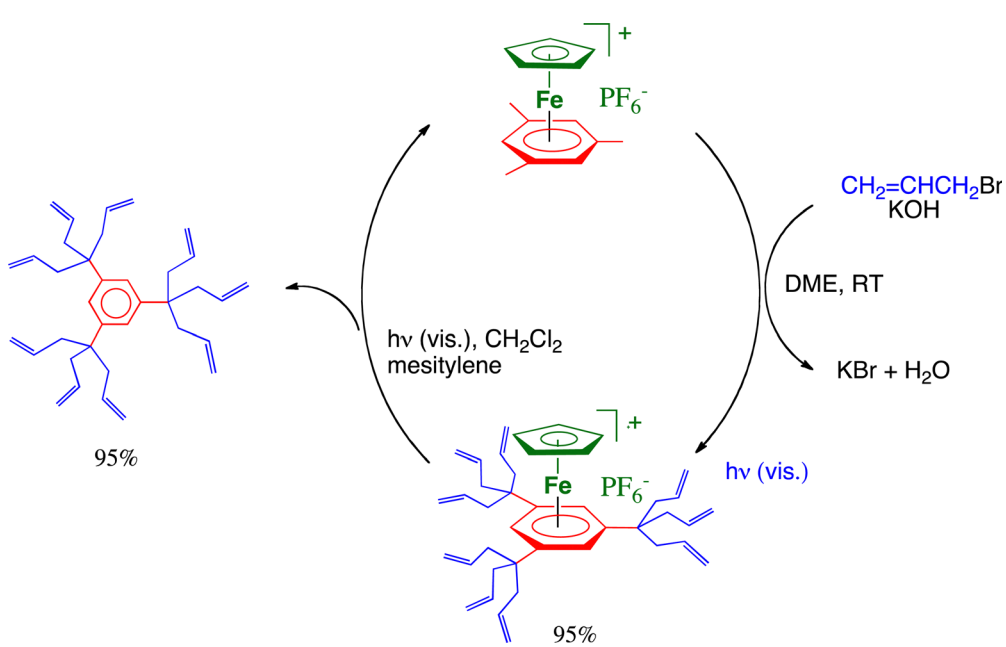
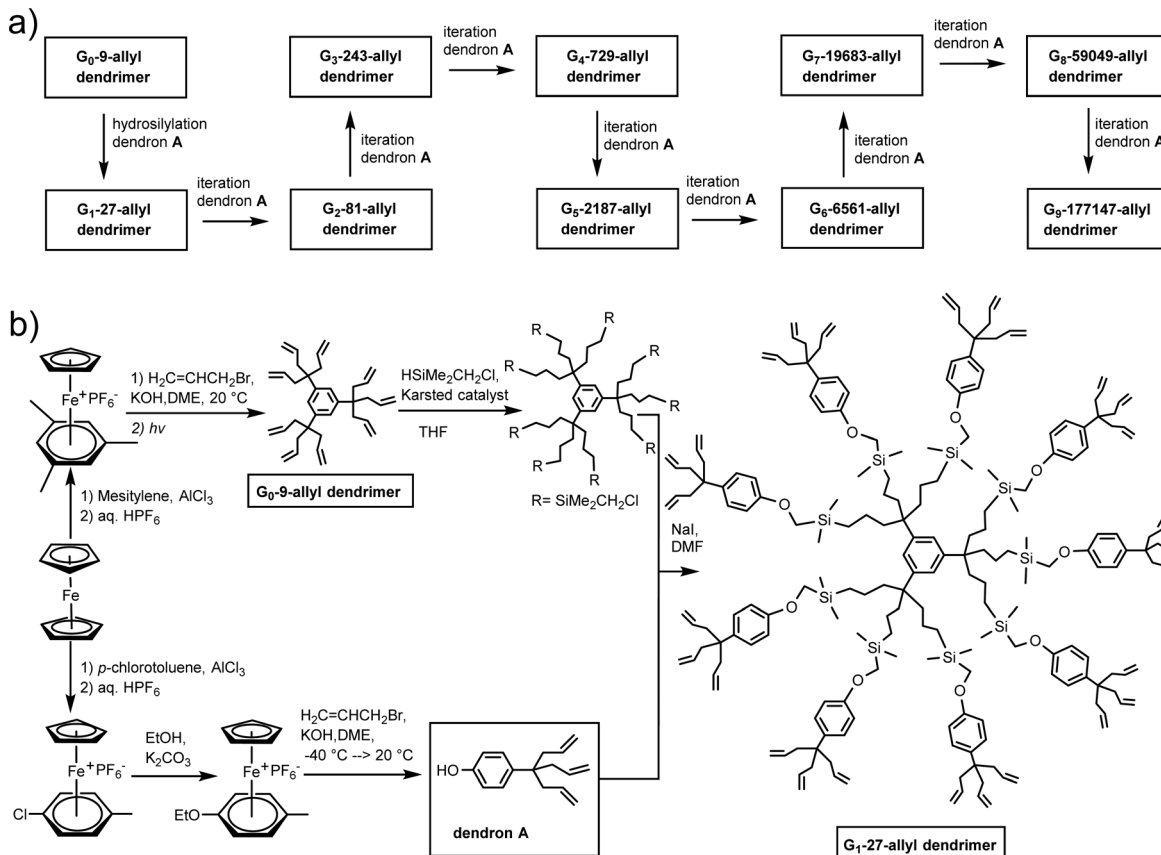


Fig. 2 Illustration of the representative properties and applications of the family of 19-electron  $\text{Fe}^{\text{I}}$  complexes **1a**, **1b** and **1c** as electron reservoirs. For the proton reservoir properties of the oxidized  $\text{Fe}^{\text{II}}$  form of these Fe sandwich complexes, see Section III.



Scheme 5  $\text{CpFe}^{\text{+}}$ -induced nona-allylation of mesitylene. The cationic charge of the  $\text{Fe}^{\text{II}}$  complex activates benzylic deprotonation by the base, followed by nucleophilic substitution of  $\text{Br}^-$  in  $\text{CH}_2=\text{CHCH}_2\text{Br}$ , this sequence proceeding 9 times *in situ* under ambient conditions. The resulting nona-allylated complex is then photolyzed by visible light in  $\text{CH}_2\text{Cl}_2$  in the presence of mesitylene to produce the iron-free nona-allylated arene, which also regenerates the starting sandwich complex of mesitylene.



**Scheme 6**  $\text{CpFe}^+$ -induced arene activation for the synthesis of the  $\text{G}_0$ -9-allyl dendritic core and dendron A towards the multiple-generation divergent construction of large poly-allyl-terminated dendrimers following 1  $\rightarrow$  3 branching until the 9th generation.

## Dendritic Size Progression

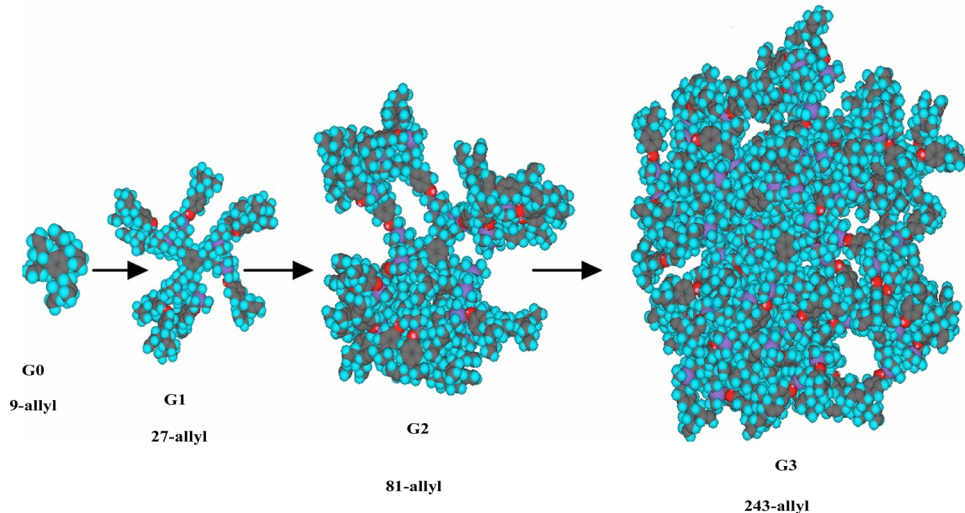


**Fig. 3** Molecular modeling of the dendritic size progression from  $\text{G}_0$  (9-allyl) to  $\text{G}_3$  (243-allyl).

complexes,<sup>54</sup> but in principle any cationic moiety in robust 18-electron complexes should be able to operate in a similar

manner. In particular, this was the case in pentamethyl- and decamethylcobalticenium and rhodicenium  $\text{PF}_6^-$  salts. In such



cases, more space is available around the permethylated  $\text{Cp}^*$  ligand ( $\text{Cp}^*=\text{C}_5\text{Me}_5$ ) for double branching than around the  $\text{C}_6\text{Me}_6$  ligand. Thus, double methylation or allylation of each exocyclic methyl group was easy, and  $[\text{CoCpCp}^*][\text{PF}_6^-]$  yielded the chiral complexes  $[\text{CoCp}(\text{C}_5\{\text{CHMe}_2\}_5)][\text{PF}_6^-]$  and  $[\text{CoCp}(\text{C}_5\{\text{CH}(\text{CH}_2\text{CH}=\text{CH}_2)_2\}_5)][\text{PF}_6^-]$ . These complexes result from double branching at each exo-cyclic carbon upon reaction with excess KOH (or *t*-BuOK) and MeI or allyl bromide, respectively. At ambient temperature, they possess a single directionality (planar chirality) of the remaining C–H bonds with full rotation only allowed (from  $^1\text{H}$  NMR) at high temperature.<sup>55,56</sup> With the decamethylcobalticenium  $\text{PF}_6^-$  salt, the reaction could not go to the end of the deprotonation–methylation sequences due to the limited space between the two rings restricting the space for the incoming groups. On the other hand, with decamethyl rhodicenium, this reaction readily gave the deca(isopropyl) rhodium complex, the only deca(isopropyl) metallocene known, because the distance between the two rings is sufficient to allow space for all these groups.<sup>57</sup>

## IV. Mixed valences, molecular electronics and molecular batteries

The late transition-metal sandwich structures afford extensive possibilities in terms of oxidation states and electron and proton transfers involving stable 17 and 19 electron complexes.<sup>58</sup> In the latter, such odd-electron non-sandwich structures, even stabilized ones, often have close energy levels and therefore involve fluxionality between these two valence states.<sup>59,60</sup> A consequence is that these sandwich and related structures provide rich mixed and average valences with controllable electronic communication between two or several metals. An early example was that of the 35-electron biferrocenium salts disclosed in 1970,<sup>61</sup> shortly following classification describing the various types of mixed-valence complexes<sup>62,63</sup> and the fine analysis by Taube of the understanding of the energetic requirements of intermetallic electron-transfer processes.<sup>64</sup> Optical properties of the biferrocenium salts indicate, due to the structural identity of both sandwiches in the

neutral states, class II mixed-valence 35-electron complexes according to the Robin-Day classification.<sup>63</sup> An example is found in the X-ray crystal structure of decamethylbiferrocenium for which the iron-ligand bond distances are distinct in the two sandwiches, indicating localization of the mixed valence in an  $\text{Fe}^{\text{II}}_2\text{Fe}^{\text{III}}$  complex.<sup>65</sup> This is not the case when two  $\text{CpFe}(\text{arene})$  units are linked through the  $\text{Cp}$  ring. The five oxidation states between the 36-electron and the 40-electron species are connected by 4 reversible cyclic voltammetry waves all separated by 0.5 V as a result of the electrostatic interactions, in a situation resembling that encountered in nanoclusters.<sup>66</sup> In this series of sandwich complexes the infrared absorption and Mössbauer spectroscopy data showed electronic delocalization, both metals being in the 1.5 oxidation state in a class-III mixed (average) valence system.<sup>67,68</sup> The other extreme with the two valence states of a fulvalene mixed-valence complex is that of the 37-electron complex  $\text{Fc-CpFe}(\text{i})\text{C}_6\text{Me}_6$  ( $\text{Fc}$  = ferrocenyl) that is clearly a localized  $\text{Fe}(\text{i})\text{Fe}(\text{ii})$  class-I mixed valence complex in the Robin-Day classification. Thus, the fulvalene bridge is extremely flexible concerning electronic communication between the two metals to which the two  $\text{Cp}$  parts of fulvalene are bound, this communication being directed by the nature of other, non-communicating (ancillary) ligands (Fig. 4).<sup>33,38,65</sup>

The reaction of 19-electron,<sup>24</sup> and also 38-electron complexes is very sensitive to the medium. For instance, if the ancillary ligand is benzene, the reaction of the 38-electron complex  $[\text{Fe}^{\text{I}}_2(\eta^{10},\mu_{2-10}\text{H}_8)(\eta^6\text{C}_6\text{H}_6)_2]$  with CO is highly dependent on the presence of a salt. Indeed, the presence of a salt such as  $\text{NaPF}_6$  in THF completely changes the fate of the reaction,<sup>18</sup> the salt-induced intramolecular electron transfer yielding the complex  $[\text{Fe}^{\text{II}}(\eta^{10},\mu_1\text{C}_{10}\text{H}_8)(\eta^6\text{C}_6\text{H}_6)]$  instead of the carbonyl-containing dimer obtained in its absence (Scheme 7). Salt-induced reactions are known to proceed upon double ion exchange between two ion pairs in molecular chemistry.<sup>18</sup> In the present case, they control intramolecular electron transfer across the fulvalene bridge.<sup>69</sup>

When two  $\text{CpFe}(\text{arene})$  units are linked by a single bond through the  $\text{Cp}$  ligands, like in Scheme 7, the cyclovoltammogram shows a single-ET cascade (arene =  $\text{C}_6\text{H}_6$  or  $\text{C}_6\text{Me}_6$ ), because the 38 e<sup>−</sup>  $\text{Fe}(\text{i})$  complex is thermally stable for

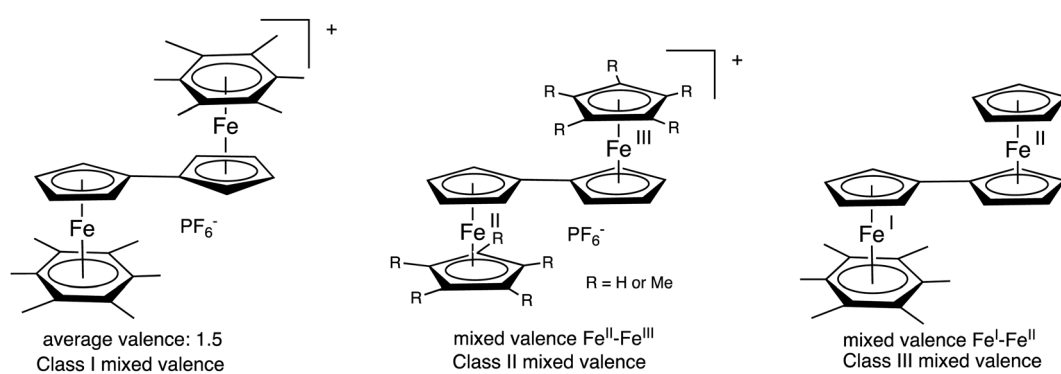
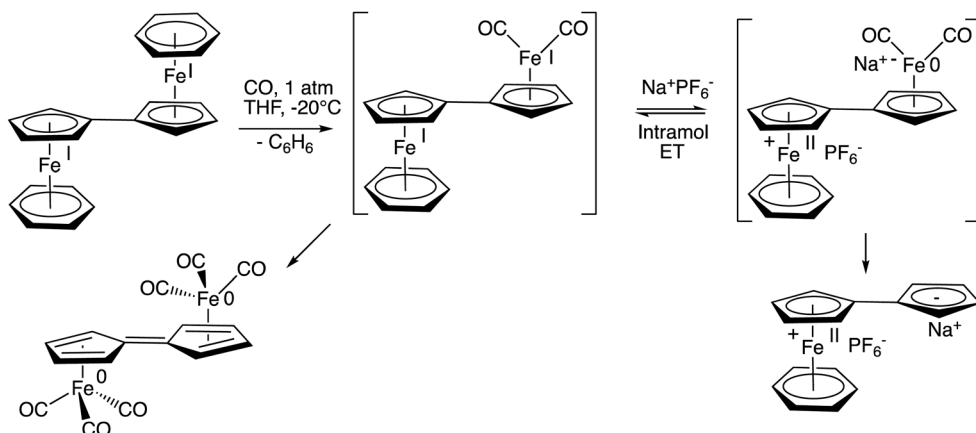


Fig. 4 Ancillary ligand-dependent electronic communication between the two metals and mixed valence type in fulvalene diiron complexes  $[\text{Fe}_2(\eta^{10},\mu_2\text{C}_{10}\text{H}_8)\text{L}_n]^{p+}$ ,  $\text{L}_n = \text{C}_5\text{R}_5$  ( $\text{R} = \text{H}$  or  $\text{Me}$ ) or  $\text{C}_6\text{Me}_6$ ,  $p = 0$  or  $1$ .<sup>65</sup>





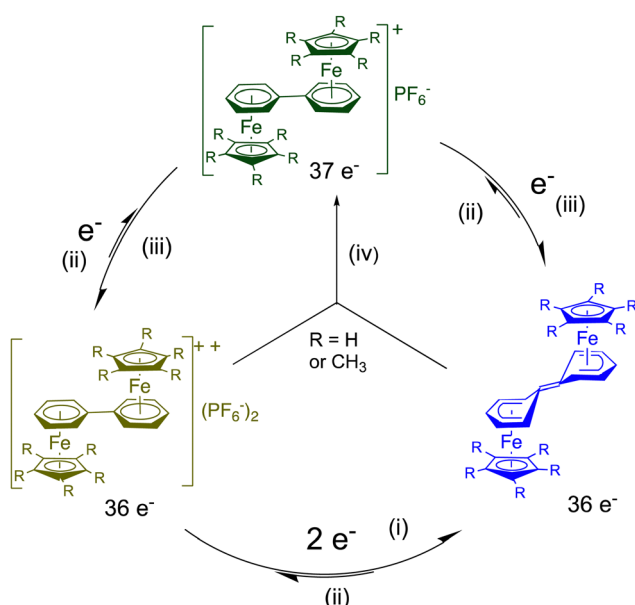
Scheme 7 Salt-induced intramolecular electron transfer between the two Fe centers across the bridging fulvalene ligand.

arene =  $C_6Me_6$ . So, this shows that, like in cluster chemistry, there is no significant reorganization along the ET cascade. On the other hand, when the two  $CpFe$ (arene) units are linked through the arene ligand in diphenyl complexes, the electronic interaction between these two virtual 19-electron iron centers is so strong that it is quenched by intra-ligand coupling into a non-planar bis-cyclohexadienylidene ligand in which the cyclohexadienyl part of each ring is bonded in a ferrocene-like pentahapto coordination mode to iron, as shown by the X-ray crystal structure of the neutral blue complex in Scheme 8 ( $R = CH_3$ ). Formally, the two incoming electrons are found in the double bond of the link, and the result is a structure isolobal to biferrocene. The driving force to reach the 18-electron, ferrocene-type structure overtakes the requirement of diphenyl aromaticity.

In the parent ( $Cp$ ) complex, the energy involved in the intramolecular coupling overtakes the electrostatic energy involved in the second single-electron reduction, and the cyclovoltammogram shows a single 2-electron wave. With the  $C_5Me_5$  analogue, this reorganization energy is a little less than the electrostatic factor, so that two close one-electron CV waves are observed, which also allows synthesizing the green average-valence 37-electron complex by comproportionation (Scheme 8). If the diphenyl group is kept rigid, however, such as in phenanthrene, triphenylene or pyrene, the cyclohexadienylidene formation is not possible.<sup>70,71</sup>

Hexa(ferrocenylethynyl)benzene, synthesized by a Negishi coupling reaction between  $C_6Br_6$  and ferrocenyl-ethynyl zinc chloride,  $FeCCZnCl$ , in the presence of the catalyst  $[Pd(PPh_3)_4]$  in refluxing THF-toluene, and methyl-substituted ferrocenyl analogues, showed interesting electrostatic and frustration effects by cyclic voltammetry (CV). With the supporting electrolyte  $N(n-Bu)_4PF_6$  in  $CH_2Cl_2$  and a platinum anode, a single six-electron CV wave was observed for hexa(ferrocenylethynyl)-benzene as well as for 1,3,5-tris(ferrocenylethynyl)benzene, but, upon using  $N(n-Bu)_4BAr_4$ , ( $ArF = 3,5-C_6H_3-(CF_3)_2$ ), three different two-electron reversible CV waves were observed for both compounds (Fig. 5).<sup>72</sup>

Since the CV of 1,3- and 1,4-bis(ferrocenylethynyl) benzene showed only one wave whatever the supporting electrolyte, it was concluded that intramolecular electronic influence among the various redox groups was not observable, because it was too weak, but CV wave splitting observed with the tris-and hexa(ferrocenylethynyl) derivatives was due to more significant electrostatic effects. In addition, the striking contrast between the behavior of the 1,3- and 1,3,5- substituted derivatives indicated that the introduction of a 3rd substituent in meta position introduced a problem. This was taken into account by the fact that, if disubstituted derivatives could adopt an anti conformation of the two ferricenium groups about the benzene plane minimizing the electrostatic repulsion between the two positive charges, such relative *anti* conformation was no longer possible upon introduction of a 3rd substituent in *meta* position, involving stereo-electrostatic frustration and the splitting

Scheme 8 Electron transfer (ET) processes of diphenyl diiron complexes of biphenyl in THF<sup>•</sup> (i)  $LiAlH_4$ ,  $-80\text{ }^\circ\text{C}$ ; (ii)  $O_2$ ,  $NaPF_6$ ; (iii)  $Na/Hg$ ,  $20\text{ }^\circ\text{C}$ ; (iv) comproportionation,  $20\text{ }^\circ\text{C}$ .<sup>70</sup> as shown by the X-ray crystal structure of the blue complex ( $R = CH_3$ ).

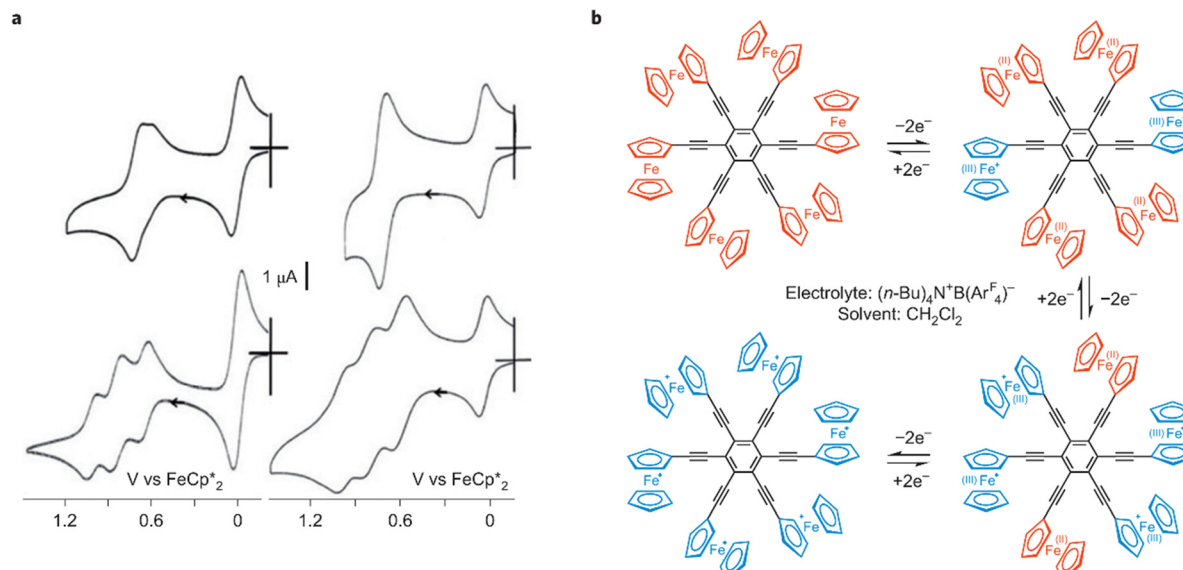


Fig. 5 Electron transfers in hexa(ferrocenylethynyl)benzene governed (similarly to 1,3,5-tris (ferrocenylethynyl)benzene) by electrostatic and conformational frustration effects in the polycationic oxidized forms. (a) Compared cyclic voltammograms of 1,3,5-tris(ferrocenylethynyl)benzene (left) and hexakis-(ferrocenylethynyl)benzene (right) in  $\text{CH}_2\text{Cl}_2$  with  $[\text{N}(n\text{-Bu})_4]\text{[PF}_6^-]$  (top) and  $[\text{N}(n\text{-Bu})_4]\text{[BAR}^{\text{F}}_4]$  (bottom,  $\text{Ar}^{\text{F}} = 3,5\text{-C}_6\text{H}_3\text{(CF}_3)_2$ ). (b) Mechanism of the oxidation of hexakis-(ferrocenylethynyl)benzene in the presence of  $[\text{N}(n\text{-Bu})_4]\text{[BAR}^{\text{F}}_4]$  0.1 N with  $\text{Ar}^{\text{F}} = 3,5\text{-C}_6\text{H}_3\text{-}(\text{CF}_3)_2$ , in  $\text{CH}_2\text{Cl}_2$ , a cascade of three two-electron oxidation steps shown in a with the CV (right, bottom). The ferrocenylethynyl groups are represented in red, whereas the ferriceniummethynyl groups are in blue; reproduced with permission from ref. 73 Copyright 2011 American Chemical Society.

of the three ferrocenyl waves. In the hexasubstituted compound, each group of two substituents in *para* substitution is equivalent, which induces the observation of 3 CV waves, as in the 1,3,5-trisubstituted derivative.<sup>72–74</sup> In large ferrocene-terminated dendrimers, these electrostatic effects become two weak to be observable, because these groups are far from one another.<sup>74</sup>

Electronic communication between two iron centers was established through a *meta* di-ethynylaryl group, providing sufficient electronic delocalization *via* this organic bridge for the stabilization of class-II mixed valency with the two iron centers.<sup>75</sup> On this basis, hexanuclear and dendritic architectures were synthesized including the class-II mixed-valence system (Scheme 9 and Fig. 6).<sup>76</sup>

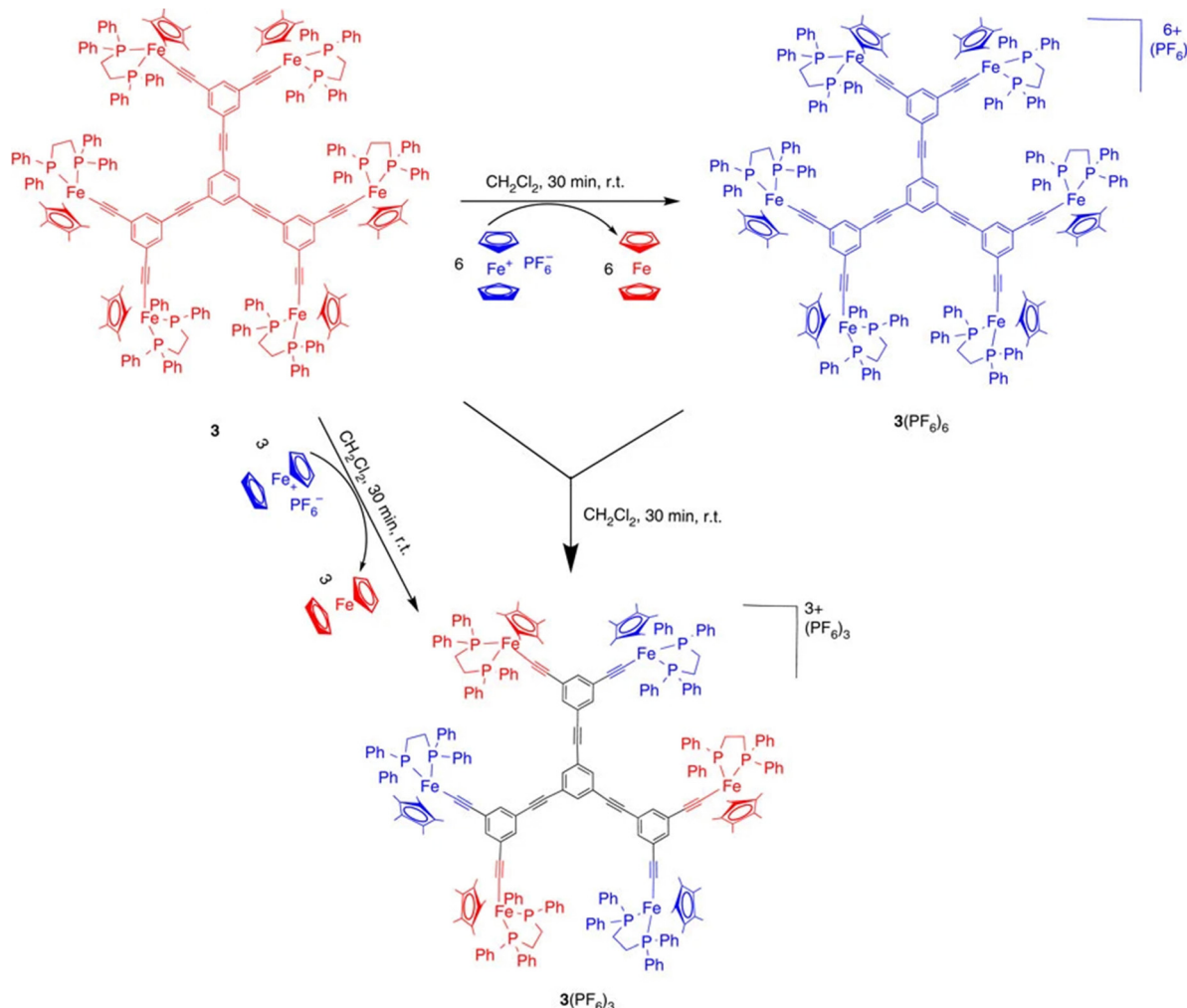
Metallopolymers containing ferrocene<sup>77,78</sup> and cobaltocene<sup>79</sup> or  $[\text{CpFe}(\text{C}_6\text{Me}_6)]^+$  units (or two or more of these metallocenes)<sup>79</sup> could be a means to target new molecular batteries.<sup>80–86</sup> Whereas ferrocene polymers have been used for some time as redox flow batteries (RFBs) because of their adequate redox potential as a catholyte (3.44 V vs.  $\text{Li}/\text{Li}^+$ ),<sup>80</sup> cobaltocenium salts have been introduced later as anolytes (1.3 V difference between the  $\text{Cp}_2\text{Fe}^{+/-}$  and  $\text{Cp}_2\text{Co}^{+/-}$  redox potentials).<sup>83</sup> Very recently, poly-ferrocenes and polycobaltocenes have efficiently been used for the first time as catholytes and anolytes, respectively in graphene oxide composites for new (RFBs). Ideal Nernstian behavior was observed up to  $>1.2 \text{ C cm}^{-2}$ , high coulombic efficiency at ultrafast rates ( $200 \text{ A g}^{-1}$ ). Charge was carried by the anion  $\text{ClO}_4^-$  upon using  $\text{Li ClO}_4$  (Scheme 10).<sup>84</sup>

The advantage of such RFBs is that electron self-exchange is fast with late metallocenes due to the fact that the metal-ligand bonds undergo only very small bond change between monocations and neutral forms (cf introduction); also, good

ion percolation is obtained upon molecular self-assembly. Upon oxidation, metallocene materials undergo size increase (breathing) due to the anion income, but this breathing is reciprocal between ferrocene and cobaltocene, cancelling the pressure built up in the closed cell that would otherwise be damaging. As a result, excellent cycling was obtained (*vide supra*).<sup>84,85</sup> Other recent studies involved charge transfer in metallocene ( $\text{FeCp}_2$  and  $\text{CoCp}_2$ ) intercalated  $\text{MoS}_2$  and  $\text{WS}_2$  and showed that the metallocene redox potentials were much dependent on the speciation and concentration of the cations in the electrolyte.<sup>86</sup> Large dendrimers also represent a viable architecture for the design of molecular batteries with metallocene-terminated dendrimers, *i.e.* either ferrocenyl or pentamethyl-ferrocenyl-terminated dendrimers (Fig. 7)<sup>87,88</sup> on one hand and metallocendrimers terminated by cobaltocenium<sup>89</sup> or  $[\text{CpFe}(\text{C}_6\text{Me}_6)]^+$  salts<sup>90</sup> on the other hand, given the equivalence of the redox centers at the dendrimer periphery.<sup>74</sup>

The equivalence of the many ferrocenyl redox sites at the dendrimer periphery for 9 generations of ferrocenyl and pentamethylferrocenyl-terminated dendrimers is shown by cyclic voltammetry (CV). Only one CV wave was observed, showing that the electrostatic factor is extremely weak, making the different redox potentials of these sites appearing equivalent. The CV waves were chemically reversible showing the stability of both  $\text{Fe}(\text{II})$  and  $\text{Fe}(\text{III})$  forms and electrochemically reversible showing fast rotation of the dendrimer bringing in turn all the redox centers near the electrode for fast electron transfer and tunneling from a ferrocene terminus to the next at the periphery.

Reversible molecular breathing between the 18-electron and the stable 17-electron oxidized forms of the metallocendrimers



**Scheme 9** Syntheses using the 17-electron ferricenium complex of both the Fe(III) and class-II mixed-valent Fe(II)–Fe(III) hexanuclear complexes. The latter can also be obtained by quantitative comproportionation between the Fe(II) and Fe(III) hexanuclear complexes. Various dendrimers containing the same mixed-valent Fe(II)–Fe(III) periphery were obtained in the same way (see Fig. 6). Blue represents Fe(II), and red, Fe(III). Reproduced with permission from ref. 76 Copyright 2014 Springer Nature.

was measured by Atomic Force Microscopy (AFM) and Electronic Force Microscopy (EFM) showing that the dendrimer size increases for the fifth generation by 50% upon oxidation and returns to the initial size upon reduction of the ferricenium form back to Fe(II) (Fig. 8).

Evidence for metal-sandwich-terminated dendrimers as electron-reservoir systems was also illustrated by single-electron transfer of each Fe(I) sandwich-terminated branch to  $C_{60}$  yielding a dendrimer with 64 positively charged Fe(II) sandwich complex, each of them electrostatically bonded to  $C_{60}^{+}$  (Fig. 9).

## V. Dendritic effect with supramolecular redox sensors of biologically important anions

Anion sensing is a major area, because anions are ubiquitous throughout biological systems (DNA, ATP, enzyme substrates and co-factors), playing a major role in medicine, catalysis, and

environment (phosphate-containing fertilizers, carcinogenesis of nitrate metabolites, pertechnetate from nuclear fuel). Anion recognition and sensing are relevant to supramolecular chemistry, because they involve weak interaction with suitable hosts.<sup>91</sup> This field has been well covered by Beer and Gale in their well-known review; the Beer group also designed families of endoreceptors linked to late transition-metal metallocenes for redox sensing.<sup>92</sup>

Molecular recognition and sensing based on metallocene-containing polymers and materials are an extended research area, mostly involving ferrocenyl compounds, that has been reviewed.<sup>93</sup> The apta-sensing strategy has recently been developed with ferrocene-labelled aptamers involving the hairpin DNA (hDNA) and linear single-stranded DNA (ssDNA) allowing simultaneous detection of multiple mycotoxins.<sup>94</sup> For instance, aptamer-target recognition enabled Fc-ssDNA to be captured at the electrode surface *via* nucleic acid hybridization. Such electrochemical sensor was assessed bioaccumulated amount of microcystin (MC)-LR in the liver and meat of fish. Herewith,



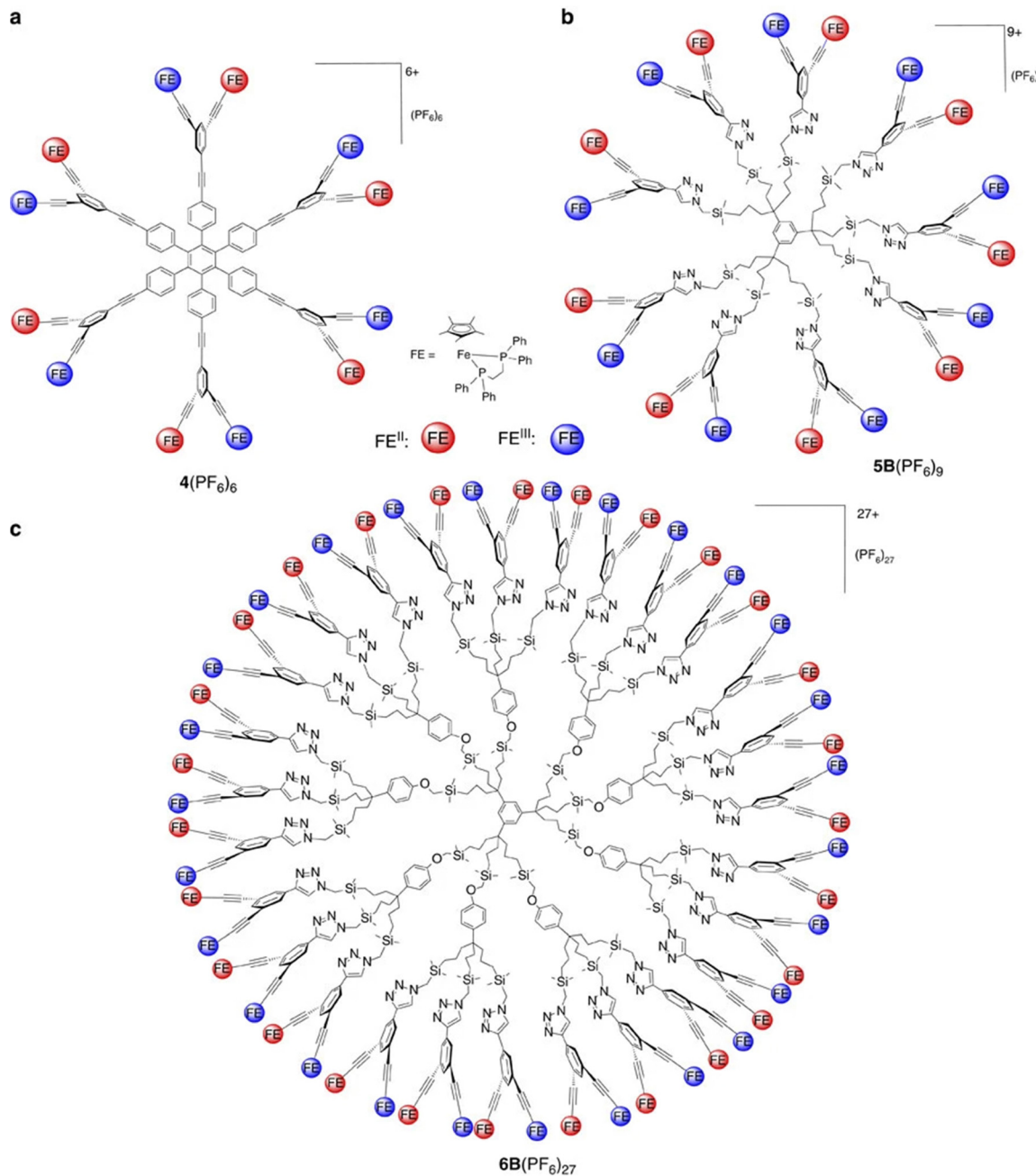


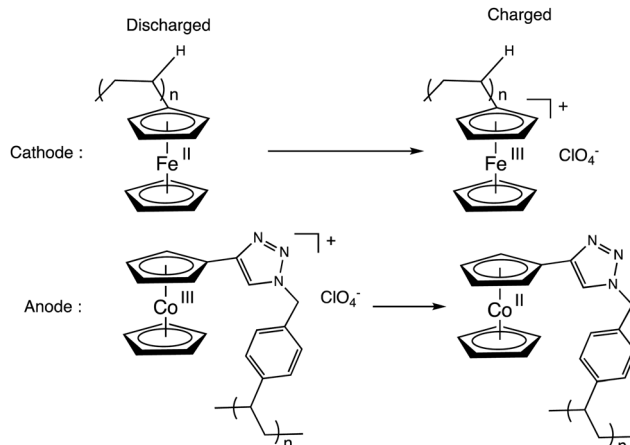
**Fig. 6** Dendritic class-II mixed valence complexes synthesized by selective oxidation with ferricinium or comproportionation as shown in Scheme 9. Reproduced with permission from ref. 76 Copyright 2016 Springer Nature.

the aptamer-based strategy was utilized to develop an electrochemical MC-LR assay toward application in MC-LR-related aquatic product safety studies.<sup>95</sup> Ferrocene-based electrochemical sensor studies are presently numerous, in particular toward electrochemical microRNAs<sup>96–99</sup> detection.

Following Beer group's sensor studies using metallocene endo-receptors,<sup>92</sup> on the other hand, ferrocene-terminated dendrimers were designed as anion exo-receptors, *i.e.* a functional group was installed next to the ferrocenyl branch termini so that its supramolecular interactions with some anions, in particular oxo anions, influence the ferrocenyl redox potential

during electrochemical titration. First successful attempts were obtained with the amidoferrocenyl-terminated dendrimers. Interestingly, it was found that the supramolecular interaction effect on the amidoferrocenyl redox potential was all the greater as the dendrimers of the same family contained a larger number of branches. This is illustrated in Fig. 10 representing a tris(amidoferrocenyl) dendron (3-Fc) and two dendrimers with 9- and 18 branches respectively (9-Fc resp. 18-Fc). In addition, a reference linear compound (1-Fc),  $[\text{Fe}(\text{C}_5\text{H}_5)(\text{C}_5\text{H}_4\text{CONH-CH}_2\text{CH}_2\text{OPh})]$ , 1-Fc, was also used for comparison. All these amidoferrocene derivatives ( $10^{-3}$  M) were titrated in an





**Scheme 10** Electrode reactions in a recent RFBs based on ferrocene polymer as catholyte and cobaltocenium salt as anolyte (driving force: 1.3 V). Electrons are transported by  $\text{ClO}_4^-$  anions.

electrochemical cell by  $n\text{-Bu}_4\text{N}^+\text{HSO}_4^-$  in  $\text{CH}_2\text{Cl}_2$  containing  $n\text{-Bu}_4\text{N}^+\text{BF}_4^-$  (0.1 M). Fig. 10 shows that 1-Fc undergoes a redox potential shift of only about 10 mV at the equivalence point, whereas **3-Fc** is shifted by 30 mV, **9-Fc** by 65 mV, and **18-Fc** by 130 mV (Fig. 10 and 11).<sup>100</sup>

There is thus a strongly positive dendritic effect. The magnitude of the redox potential shift varied as follows with the nature of the anion:  $\text{H}_2\text{PO}_4^- > \text{HSO}_4^- > \text{Cl}^- > \text{NO}_3^-$ .

The chemical reversibility of the redox site is even strengthened upon using the permethylated ligand  $\text{C}_5\text{Me}_5$  ( $\text{Cp}^*$ ) in the ferrocenyl group,<sup>101,102</sup> which is also useful for ferrocene-based dendritic batteries.<sup>80,87,88</sup> The reasons for these redox potential shifts are (i) the H-bonding interaction between the amido group and the anion, (ii) the electrostatic attraction between the positively charged ferricenium form in the course of electrochemical anodic scanning and the anion and (iii) the dendritic confinement effect provoked by the congestion between branches offering only a narrow channel to the anion for interaction that is all the more marked as the dendrimer generation is higher. Note that the two first effects are very small in a linear compound, and it is the third endo- or exo-receptor effect that very much increases the two first factors (Fig. 12).

The binding constant between the dendritic host and the anion is much larger in the cationic ferricenium form ( $K_+$ ) than in the neutral ferrocene form ( $K_0$ ) due to the additional electrostatic interaction in the cationic form. The constant ratio is accessible from the difference between the redox potentials observed without interaction with the anion (beginning of titration) and that with full interaction (end of titration) as follows,  $K_0$  being then reached by  $^1\text{H}$  NMR (Scheme 11):<sup>103</sup>

$$E_{\text{free}}^{\circ} - E_{\text{bound}}^{\circ} = \Delta E^{\circ}(\text{V}) = 0.059 \log(K_+/K_0) \text{ at } 25^{\circ}\text{C}.$$

A variety of redox sites, functional links and receptors have been designed.<sup>92-110</sup> Redox sites of the  $[\text{FeCp}(\text{arene})]$  family are also excellent choice, because the  $\text{Fe}^{\text{II}}/\text{I}$  redox system is often

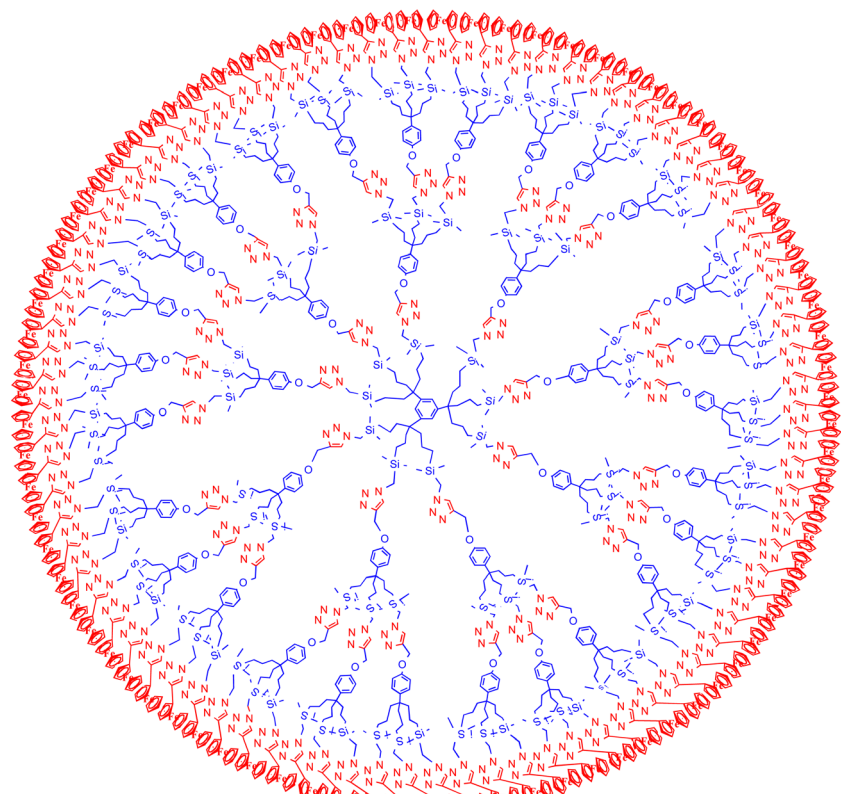


**Fig. 7** Planar representation of an 81-ferrocene dendrimer, with equivalent terminal groups, that can serve as battery catholyte.



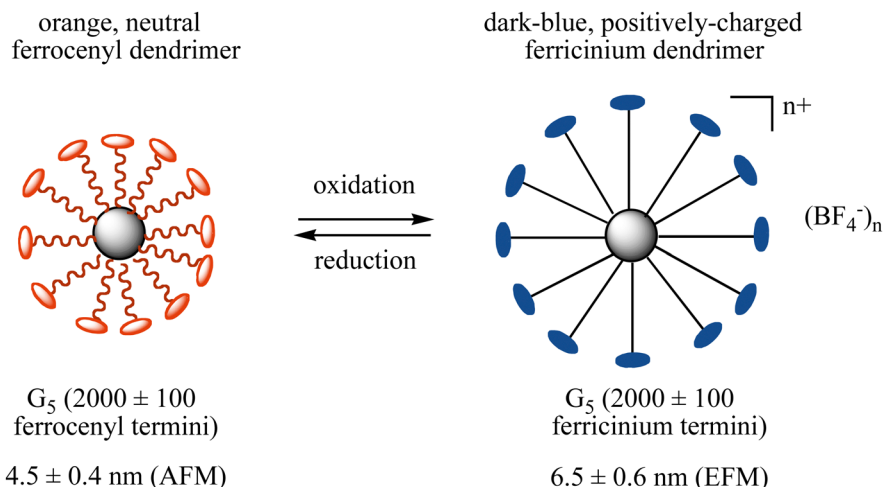


Fig. 8 Redox breathing of a 5th generation ferrocenyl-terminated dendrimer constructed according to Scheme 6 followed by the reaction of  $G_5\text{-CH}_2\text{I}$  with  $\text{Fc}(\text{CH}_2)_{11}\text{O}-p\text{-C}_6\text{H}_4\text{OH}$  in the presence of  $\text{K}_2\text{CO}_3$  in DMF for 2 d at  $80^\circ\text{C}$ .<sup>87</sup>

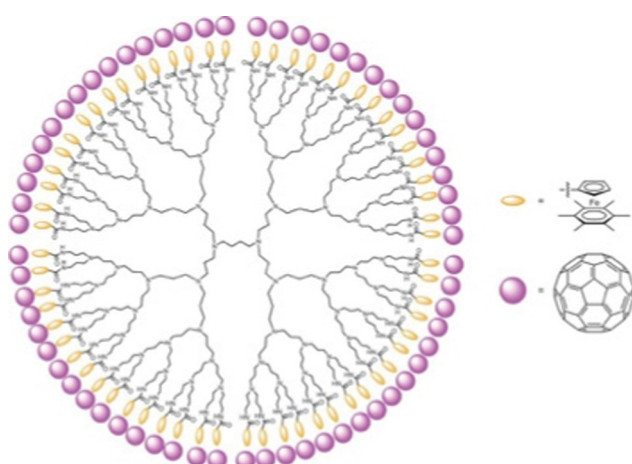


Fig. 9 Dendri-64[-NHC(O)-CpFe(II)<sup>+</sup>C<sub>6</sub>Me<sub>6</sub>C<sub>60</sub><sup>•-</sup>] (with Dendri = diamino-butane (DAB)-core  $G_5$  dendrimer) from the reaction between Dendri-64[-NHC(O)-CpFe(II)<sup>+</sup>C<sub>6</sub>Me<sub>6</sub>] with 64 equiv. C<sub>60</sub>. EPR:  $g = 2.00093$ ,  $\Delta H = 3.12$  G. Reproduced with permission from ref. 74. Copyright 2012 Springer Nature.

chemically and electrochemically reversible in this series. For instance, dendrimers terminated with  $[\text{FeCp}^*(\eta^6\text{-C}_6\text{H}_5\text{NH})]$  are excellent redox sensors for  $\text{Cl}^-$  and  $\text{Br}^-$ .<sup>106</sup> Oxo anions deserve special attention, because genetic materials contain phosphate derived anions. Gold NP-centered amidoferrocenyl-terminated stars showed excellent oxo-anion sensing properties,<sup>108,109</sup> and gold NP-centered silylferrocenyl-terminated dendrimers were selective  $\text{ATP}^{2-}$  sensors (Fig. 13).<sup>109</sup>

Even dendrimers that are not assembled with covalent bonds, but supramolecularly assembled with a core and H-bonded dendrons are efficient and selective for oxo-anion sensing (Fig. 9).<sup>110</sup> The dendritic topology with its dendritic effect represents an advantage over polymers or co-polymers, however, for  $\text{ATP}^{2-}$  sensing with the same amido linker (Fig. 14 and 15).<sup>109</sup> These macromolecular sensors are easily adsorbed on Pt electrodes upon scanning around the potential of the

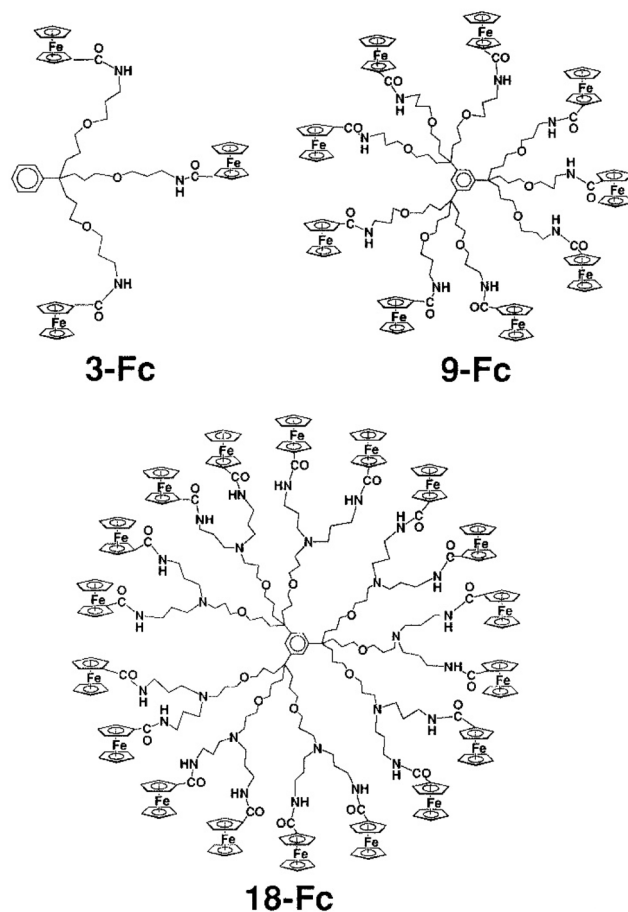


Fig. 10 Metallocendrimers with 3 (3-Fc), 9 (9-Fc) and 27 (18-Fc) terminal amidoferrocenyl groups that recognize oxo-anions using cyclic voltammetry, CV (see Fig. 11). Reproduced with permission from ref. 100. Copyright 1997 American Chemical Society.

redox site, and the modified Pt electrode sensors are easily washed from substrate after sensing toward the next run.



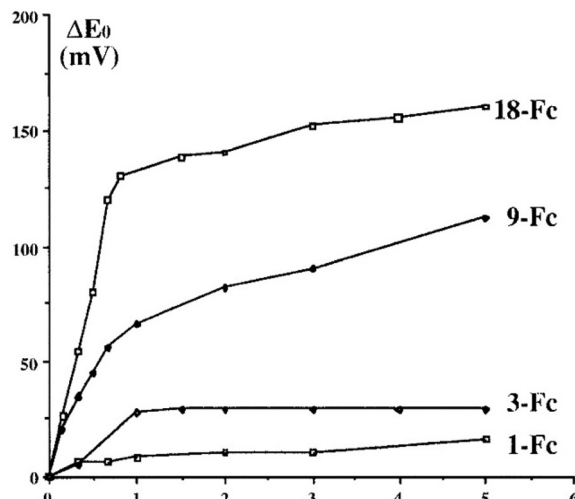
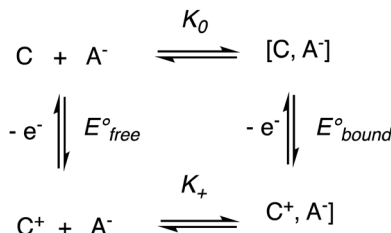


Fig. 11 Dendritic effect for redox sensing of oxoanions: example of  $\text{HSO}_4^-$ . Number of equiv. of  $n\text{-Bu}_4\text{N}^+\text{HSO}_4^-$  added per branch. Titration of 1-Fc (1-Fc)  $[\text{Fe}(\text{C}_5\text{H}_5)(\text{C}_5\text{H}_4\text{CONHCH}_2\text{CH}_2\text{OPh})]$ , 3-Fc, 9-Fc, and 18-Fc (see Fig. 10) by  $n\text{-Bu}_4\text{N}^+\text{HSO}_4^-$  monitored by CV. Concentrations in FcDs were 0.001 M,  $\text{CH}_2\text{Cl}_2$ ,  $n\text{-Bu}_4\text{N}^+\text{BF}_4^-$  (0.1 M), 20 °C, reference electrode: SCE, auxiliary and working electrodes: Pt, scan rate: 100 mV s<sup>-1</sup>. Reproduced with permission from ref. 100. Copyright 1997 American Chemical Society.



Scheme 11 Square scheme showing the association constant  $K_0$  between the ferrocenyl dendrimer and the anion and that between the oxidized dendrimer and the anion ( $K_+$ ) as a function of the redox potentials of the ferrocenyl dendrimer alone before titration ( $E^{\circ}_{\text{free}}$ ) and in the presence of the anion at the end of titration ( $E^{\circ}_{\text{bound}}$ ). If  $K_0$  is large (strong association of  $\text{A}^-$  with the ferrocenyl dendrimer), the second cyclovoltammetry wave appears during the titration. If  $K_0$  is small (weak association), the unique wave progressively shifts during the titration upon addition of the anion salt.

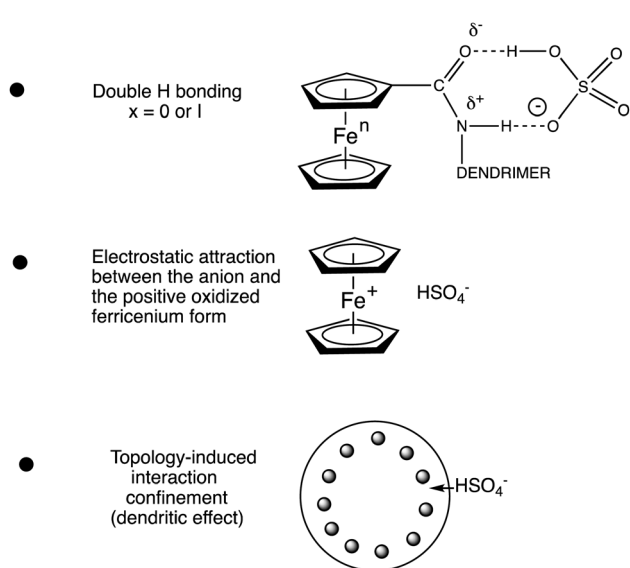


Fig. 12 The three effects responsible for the redox recognition of anions.

Another useful link between the redox site and the receptor for redox sensing application in dendrimers<sup>111–119</sup> and functionalized gold<sup>120</sup> and palladium nanoparticles<sup>121</sup> is the 1,2,3-triazole function formed by Cu(I) azide alkyne catalyzed (CuAAC) click reaction<sup>111–119</sup> either between azido-terminated dendrimers and alkynyl-ferrocene<sup>111–121</sup> or between alkynyl-terminated dendrimers and azido ferrocene<sup>122,123</sup> (Scheme 12).

Ferrocenyl (or cobaltocenyl) triazolyl dendrimers are good sensors for both oxo-anions with supramolecular interactions

connected via the triazole N atoms and for transition metal cations through binding to the triazole as ligand.<sup>107–109</sup> The single CV wave observed for all the ferrocenyl groups facilitates sensing, as their number was determined using the Bard–Anson equation using the redox system  $[\text{FeCp}^*_{2+}/0]$  as a reference.

For the oxo anions ( $n\text{-Bu}_4\text{N}^+(\text{H}_2\text{PO}_4^-)$  or  $(n\text{-Bu}_4\text{N})_2(\text{ATP})$ ), the new redox wave is located at a less positive potential than the initial wave, because the dendrimer–oxo anion assembly is easier to oxidize than the dendrimer alone with the anion donating electron density to the redox system. For transition metal cations, the new CV wave appears upon titration at a more positive potential than the initial wave, because the cation-dendrimer assembly is more difficult to oxidize than the initial redox center due to electron-releasing coordination of the triazole ligand to the added metal cation. This molecular redox recognition is all the larger (difference in redox potential upon ion salt addition) as the dendrimer generation is higher, in accord with the positive dendritic effect in redox sensing.

A remarkable case is that of the click triazolylbiferrocenyl-terminated dendrimers that can recognize both oxo-anion from the terminal ferrocenyl groups oxidized first because they are more electron-rich than the inner ferrocenyl groups, and metal cations through coordination to the triazolylferrocenyl group, a sensor system that can be installed onto a Pt electrode to modify it upon scanning (Fig. 16 and 17).<sup>109</sup>

## VI. Dendrimers and ferrocene-containing macromolecular devices in biomedicine

Ferrocene and dendrimers have long been the subjects of focuses due to their biomedical properties. Since the finding in 1971 of the properties of ferrocenone (*o*-sodium carboxylate benzoyl ferrocene, Fig. 18, left, the only ferrocenyl drug so far approved for clinical use) against anemia<sup>124</sup> and the first discovery and investigation in 1978 of ferrocene derivatives as anti-cancer drugs,<sup>125</sup> ferrocene-containing substrates have

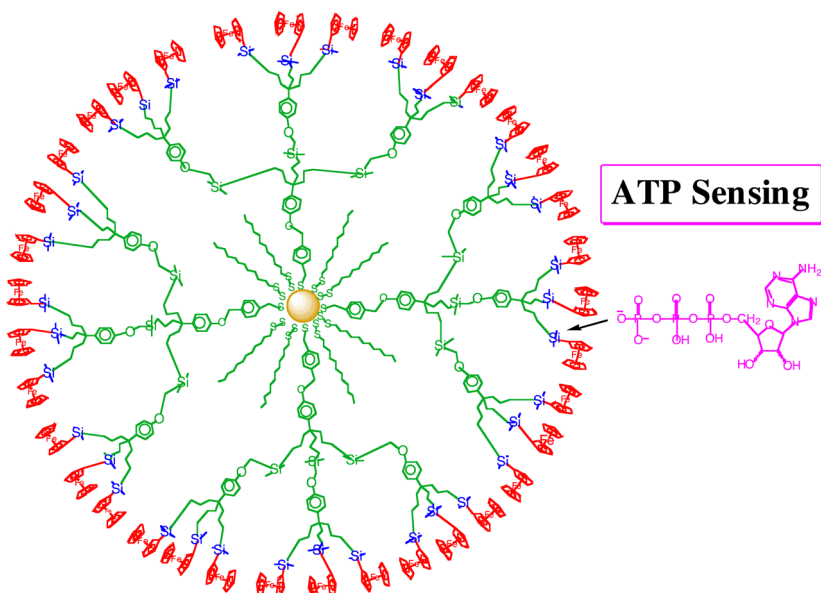


Fig. 13 ATP anion redox sensing by gold NP-centered silylferrocenyl-terminated dendrimers (planar representation). The oxygen ATP atoms interact with the electrophilic Si atoms.

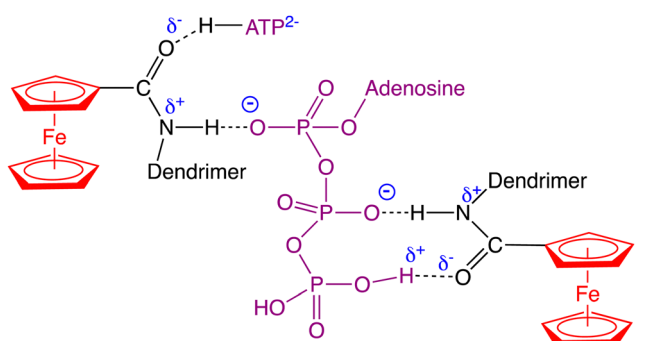


Fig. 14 Supramolecular (H-bonding) interactions between  $\text{ATP}^{2-}$  with amidoferrocenyl termini of dendrimers allowing to sense  $\text{ATP}^{2-}$ .

constantly been investigated for their anti-cancer and other biomedical properties.<sup>126–129</sup> The other most advanced drug in clinical trials, ferroquine (Fig. 18, middle), is in phase IIb of clinical trials for its anti-malarial activity *in vivo*, in combination with artesunate (a fast-killing antiparasitic trioxolane).<sup>128</sup> A good example of ferrocene-containing anti-tumoral drug is the ferrocifen family (Fig. 18, bottom, right) for which the ferrocenyl group replaces the phenyl group of the anticancer drug tamoxifen.<sup>129</sup> The strength of all the ferrocene-containing drug candidates is their ability to produce reactive oxygen species (ROS) such as  $\text{OH}^\bullet$  near cancer cells where  $\text{H}_2\text{O}_2$  is present, using ferrocene redox chemistry in Fenton-type reactions (Fig. 18(a)).

Therefore, a 80 nm-size nanozyme Co-ferrocene metal-organic framework combining glucose oxidase was reported to function as enzymatic/Fenton catalytic platform generating gluconic acid and  $\text{H}_2\text{O}_2$  resulting in excellent Fenton effect for

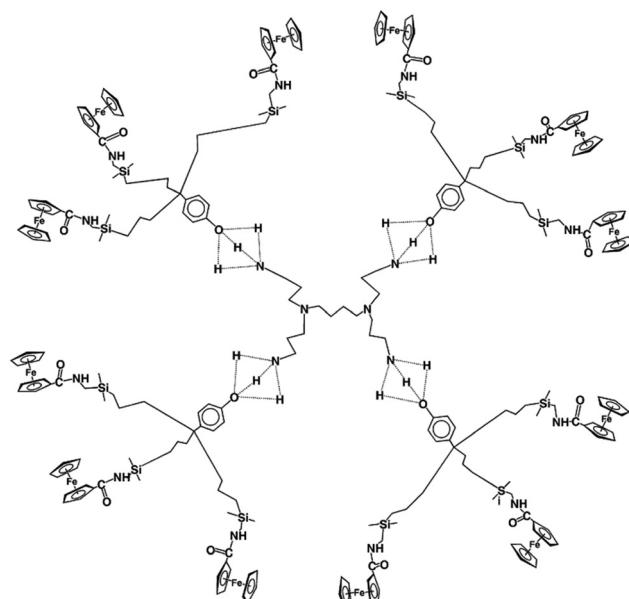
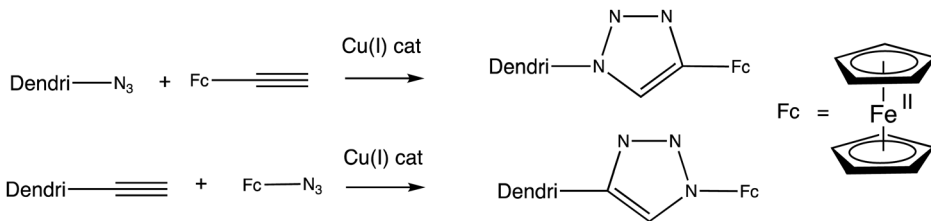


Fig. 15 Arbitrary representation of the reversible hydrogen bonding between  $\text{G}_1\text{-DAB-dend-(NH}_2)_4$  and a triamidoferrocenyl dendron shown by the concentration-dependent average location of the (broad)  $\text{NH}_2 + \text{OH}$  signal in  $^1\text{H}$  NMR between 2.4 and 4.1 ppm vs. TMS in  $\text{CDCl}_3$ .

the generation of highly toxic  $\text{OH}^\bullet$  radicals remarkably increasing tumor treatment.<sup>130</sup>

The incorporation of metal-containing artificial analogues into DNA strands has been reported to control the size and the functions of noncanonical self-assemblies of multifunctional DNA nanostructures, assembled from long DNA building blocks, and named DNA nanoflowers. The introduction of a



Scheme 12 Two ways to branch a redox site with a 1,2,3-triazole to a dendritic receptor.

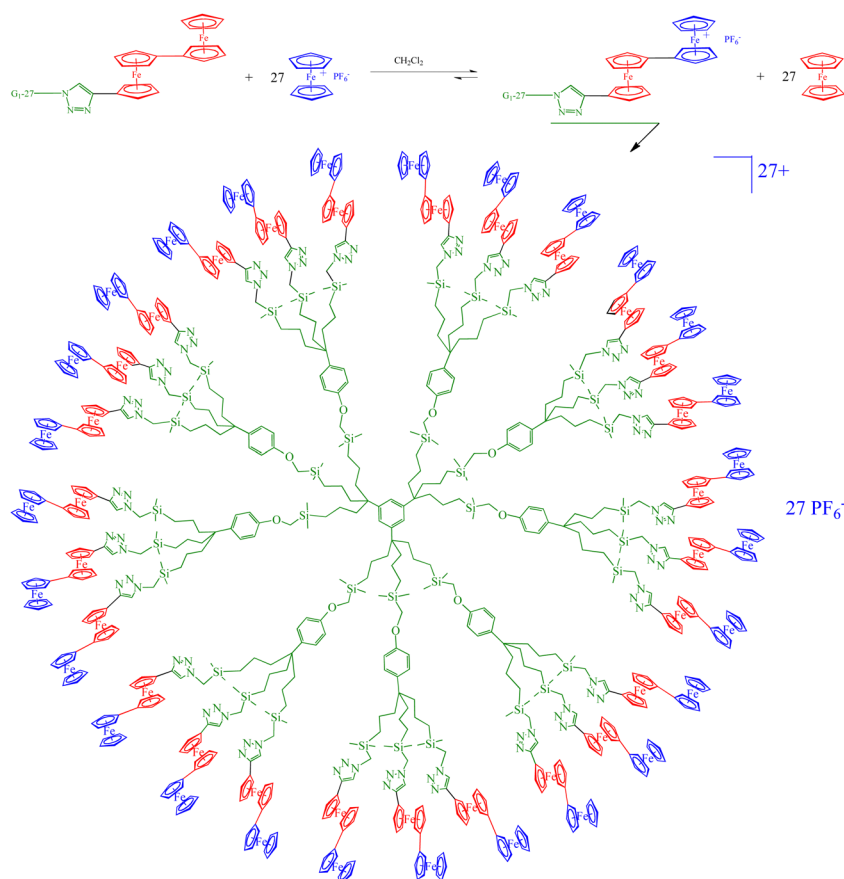


Fig. 16 Selective oxidation of the outer ferrocenyl groups (blue) in the 27-biferrocenyl dendrimer.

ferrocene (Fc) base allowed size controllability and self-degradability of Sgc8-NFs-Fc with  $\text{H}_2\text{O}_2$  *via* Fenton's reaction.<sup>131</sup> Amphiphilic polymer micelles formed by self-assembling arachidonic acid and azobenzene linked to Fc was shown to be an effective cell carrier and expected to develop in sensitizing ferroptosis (programmed cell death pathway) and anti-tumor.<sup>132</sup> An Ir(III) complex liganded to a ferrocene-modified diphosphine that localizes in lysosomes also showed ferroptosis effective for cancer immunotherapy.<sup>133</sup>

Dendritic macromolecules have long been another area of interest for a wide variety of biomedical applications,<sup>134–139</sup> because of their capacity of drug encapsulation.<sup>129,140</sup> An example from our group is docetaxel (Fig. 19), commercialized as taxotere (from the taxoid antineoplastic family), and

discovered in 1989 by Pierre Pottier and his group at the ICSN institute of Gif-sur-Yvette, near Paris, upon hemi-synthesis from 10-deacetylbaicatin-III extracted from the leaves of the European yew (*Taxus baccata*).<sup>141</sup> It is registered in the updated Model List of Essential Medicines by the World Organization of Health (WHO).

Docetaxel is very efficient against breast, lung and metastatic prostate cancers by stabilizing the microtubules upon inhibition of their depolymerization by stable bond formation with its cellular receptor, tubulin, which generates the blockade of mitosis. Docetaxel nanotechnology in anti-cancer therapy is essential towards the vectorization of the drug in order to optimize its efficiency and minimize side effects.<sup>141,142</sup> Therefore, docetaxel, that is hydrophobic, insoluble in water,



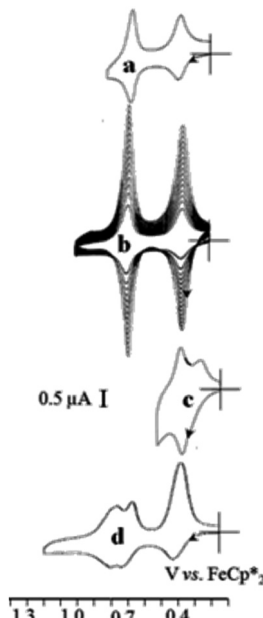


**Fig. 17** Selective roles of the inner and outer ferrocenyl redox centers of the 81-biferrrocenyl dendrimer in the redox recognition of  $\text{ATP}^{2-}$  and  $\text{Pd}^{2+}$ . Cyclic voltammograms of the G2-81-biferrrocenyl click dendrimer, (a) in  $\text{CH}_2\text{Cl}_2$ ,  $[\text{n-Bu}_4\text{N}][\text{PF}_6]$  0.1 M; (b) progressive adsorption upon scanning around the potential of the biFc area; (c) splitting of the outer-Fc CV wave at 0.4 V upon addition of  $[\text{ATP}][\text{n-Bu}_4\text{N}]_2$ ; (d) addition of  $\text{Pd}(\text{OAc})_2$  provoking the splitting of the inner-Fc wave at 0.7 V. Reproduced with permission from ref. 117. Copyright 2010 Wiley-VCH.

was solubilized upon encapsulation into dendrimer-like PEGylated gold nanoparticles, which allowed recording its  $^1\text{H}$  NMR spectrum in  $\text{D}_2\text{O}$  (Fig. 20). This encapsulation of docetaxel was utilized for its vectorization to cancer cells, which was achieved with positive *in vitro* results.<sup>143</sup>

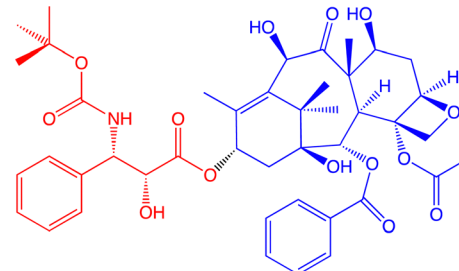


**Fig. 19** Structure of docetaxel (formulated as taxotere). The red part was added upon hemi-synthesis from 10-deacetylbaicatin-III (blue part) extracted from the European yew leaves.<sup>141</sup>

As opposed to the long-known aggregation-caused quenching (ACQ) of light emission in the condensed phase due to decay *via* non-radiative pathways of aggregate excited states,<sup>144</sup> Tang discovered in 2001 the phenomenon of aggregation-induced emission (AIE) that he assigned to restriction of intramolecular rotation (RIR) inhibiting non-radiative decay.<sup>145</sup> Tang extended the concept to collective intra- and inter-chain  $n \rightarrow \pi^*$  interactions of heteroatoms and to various other types of macromolecules.<sup>146–148</sup> Along this line and following the emission properties of dendrimers, Tomalia later proposed that, similar to RIR, restricted intramolecular mobility (RIM) in dendrimer structure due to aggregation of numerous non-emissive, electron rich, heteroatomic groups was a source of AIE named non-traditional intrinsic luminescence (NTIL).<sup>149,150</sup> Merging dendrimer and ferrocene properties towards theranostic applications was a recent target of our group in collaboration with the Ornelas group, particularly because dendrimers containing some functions can undergo AIE. Indeed, triazolylferrocenyl dendrimers of the family of that shown in Fig. 7 self-assembled into nanovesicles and vesosomes in water (Fig. 21) and presented green NTIL

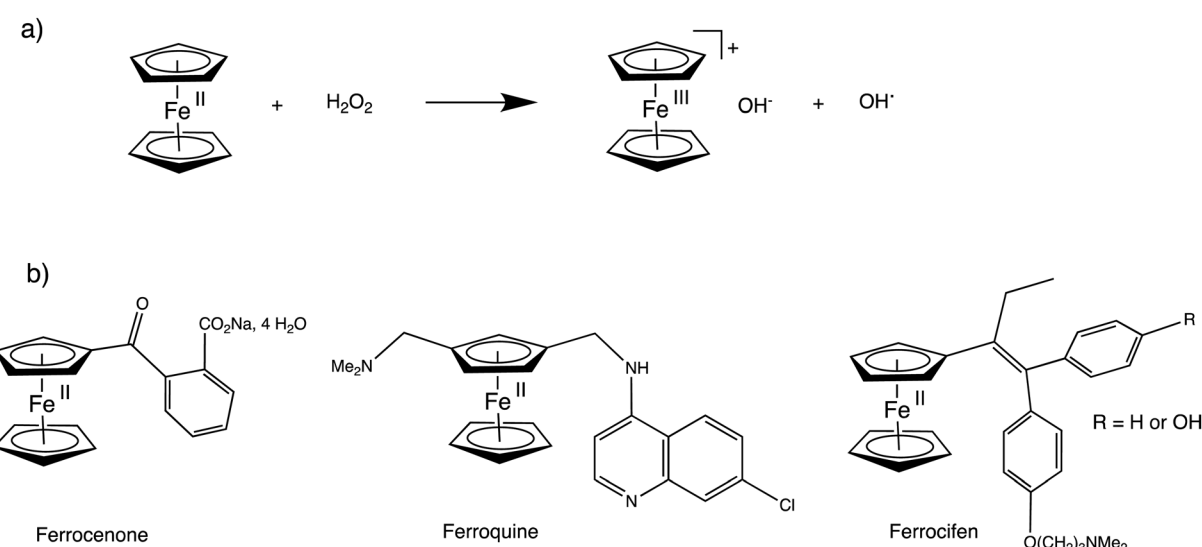


**Fig. 18** (a) Fenton-type reaction of ferrocene partly responsible for ferrocene drug activity upon generating  $\text{OH}^\bullet$  radicals at the vicinity of the sick cells; (b) main types of ferrocene-containing drugs.

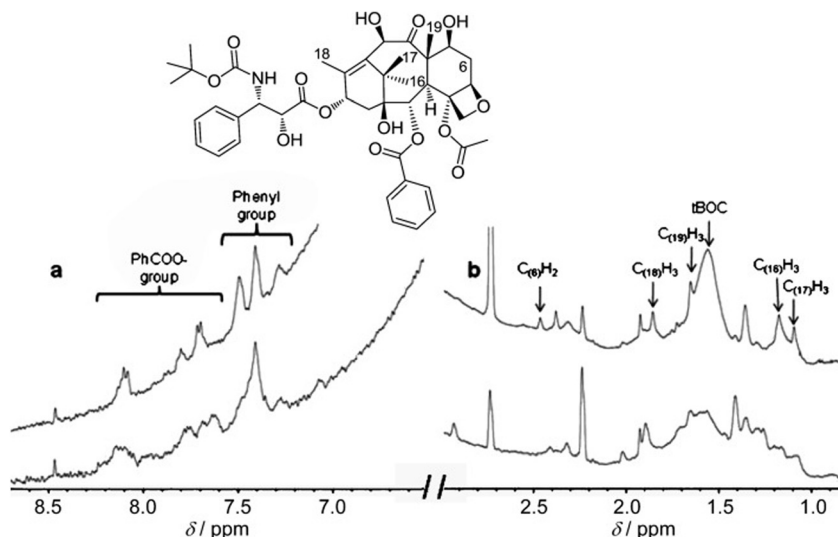


Fig. 20  $^1\text{H}$  NMR spectroscopic (600 MHz) analysis (a)  $> 6$  ppm and (b)  $< 3$  ppm of AuNP-encapsulated docetaxel (9.5 molecules per Au atom) in  $\text{H}_2\text{O}$ . Upper traces: docetaxel only; lower traces: docetaxel-AuNPs. Signal assignments were carried out by comparison with the spectrum in DMSO. Note that the solubility of docetaxel alone in  $\text{H}_2\text{O}$  is by far too low to record a spectrum in this solvent without AuNPs. Reproduced with permission from ref. 143. Copyright 2011 Wiley-VCH.

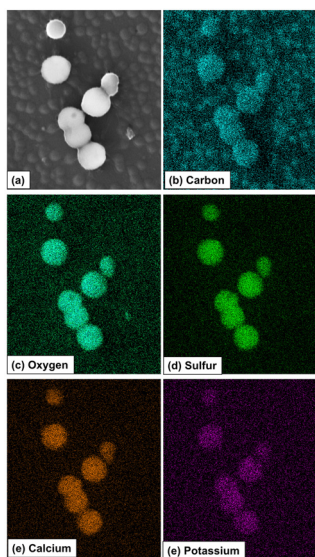


Fig. 21 SEM/EDS elemental mapping profiles of the vesosomes resulting from self-assembling triazolylferrocenyl dendrimers in water. Reproduced from ref. 151. Copyright 2021 American Chemical Society.

fluorescence and cytotoxicity allowing the development of new theranostic systems.<sup>151</sup>

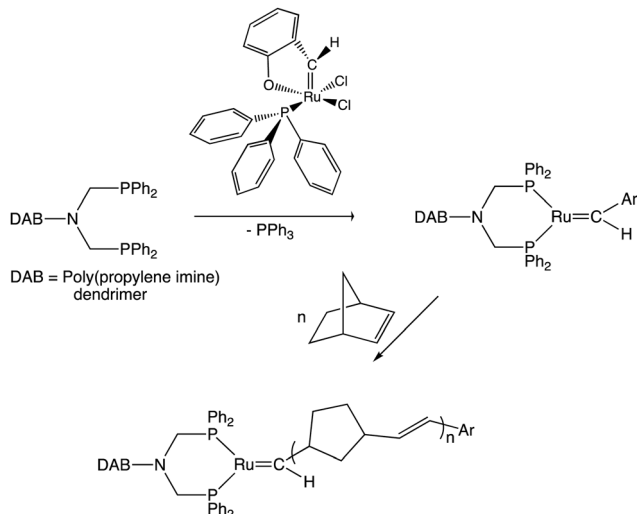
Several generations of our triazolylferrocene-terminated dendrimers of the family shown in Fig. 7 contain numerous ether, silyl and triazoly heteroatoms and therefore could lead to such “hybridized assemblies of single quantum state-like clouds of delocalizable electrons”.<sup>150</sup> The location of large ferrocene groups at the dendrimer periphery contributes to restricting intradendritic motion responsible for enhancement of emission.

## VII. Olefin metathesis reactions with dendrimers and application to soft materials

The discovery of efficient olefin metathesis polymerization catalysts has been a considerable breakthrough towards new functional macromolecules.<sup>152–154</sup> In our group, for instance, an early example consisted in adapting such a catalyst at the periphery of several generations of poly(propylene imine) (so-called DAB) dendrimers, then polymerize norbornene using these dendritic Ring-Opening Metathesis Polymerization (ROMP) catalysts, which produced giant DAB-dendrimer-cored macromolecules (Scheme 13). Remarkably, the polymerization rates were higher for the dendrimers than with a monomer propylene imine-derived ruthenium catalyst, possibly because steric congestion among the ruthenium ligands of the catalyst, but the rates decreased as the dendrimer generation increased. Indeed, with catalysts located at dendrimer peripheries, we usually observed a negative dendritic effect (*i.e.* decreased rates as the dendrimer generation increased) due to steric bulk inhibiting substrate approach to the catalytic center, which was opposite to redox sensors for which the dendritic effect was always positive.<sup>155</sup>

The nona-allyl dendrimer core obtained in Scheme 6 from mesitylene was the subject of remarkably selective olefin metathesis reactions catalyzed by Grubbs's second-generation catalyst,  $[\text{Ru}(\text{=CHPh}) (\text{NHC})\text{Cl}_2]$ . Ring Closing Metathesis (RCM) of two of the three allyl group of each triallyl tripod was fast, giving a cyclopentenyl substituent. On the other end, the reaction of the third allyl group of each tripod was much slower and depended of the reaction conditions (Scheme 14).<sup>156,157</sup>

In the presence of an acrylic ester, cross metathesis with this functional olefin allowed substrate functionalization, but, in its



**Scheme 13** ROMP of norbornene ( $n = 100$ ) at the periphery of 3 generations ( $G_1$ ,  $G_2$  and  $G_3$ ) of DAB dendrimers producing giant dendritic-cored star-shaped macromolecules using a ruthenium benzylidene catalyst. In the dendrimers of this scheme, the Ru benzylidene ligand is simplified as  $=\text{CHAr}$  and the chloro ligands are omitted for clarity. The dendritic DAB-cored phosphines were accessible by reactions of the first, second and third generation DAB dendrimers with  $\text{P}(\text{Cl})\text{Ph}_2$ .

absence, slow triple cross metathesis with another molecule yielded a single capsule compound as the thermodynamic end-product assembling two arene moieties. Many intermediate oligomers were observed by MALDI TOF mass spectrometry as kinetic products in this latter reaction. Lengthening the tethers before metathesis highlighted the interest of the cross metathesis for the functionalization of olefin-terminated dendrimers with acrylic acid and esters, as illustrated in Scheme 15.<sup>157</sup>

Another useful aspect of ferrocene or cobaltincium-containing macromolecules concerns metallohydrogels. Supramolecular gels are soft materials composed of small gelator molecule assembled into supramolecular networks, with space filled by solvent. Some gel materials are able to respond to various stimuli including with redox groups such as ferrocene, making them attractive drug delivery vehicles and as matrices for tissue regeneration.<sup>158,159</sup> Immobilization in the hydrogel of glucose oxidase (GOx) modified with ferrocene produces an electrically contacted enzyme electrode that stimulates the bioelectrocatalyzed oxidation of glucose. Upon incorporation of a load into the hydrogel, the electrocatalyzed oxidation of glucose and the accompanying acidification allow controlling the release of the load.<sup>160</sup> Hydrogels that contained dendritic and polymeric ferrocene ensembles synthesized using the ROMP technique with the same Grubbs-II catalyst in macromolecular di-block assemblies allowed access to self-healing materials for biomedical applications including redox-stimuli-responsive drug delivery systems.<sup>161</sup> Examples of the encapsulation/release of substrates include rhodamine, benzocain and the anti-cancer drug doxorubicin upon redox switch with suitable redox reagents of the ferrocene unit in metallopolymer micelles (Fig. 22).<sup>161–164</sup>

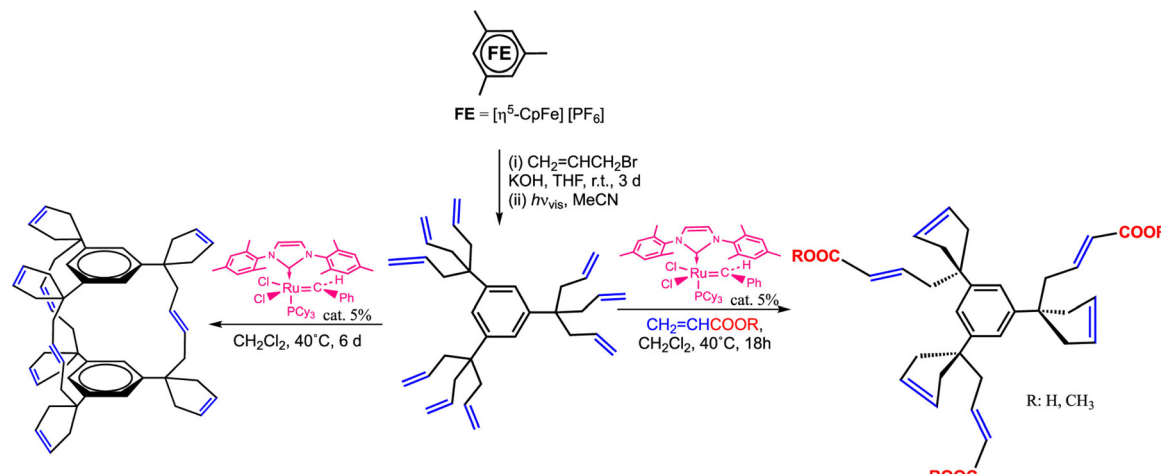
Supramolecular soft-templating mesoporous materials have been reported to allow regulating uniform pore structure with designed dimensions hosting *situ* synthesis of nano-objects toward applications for separation, sensing, catalysis, energy conversion and storage, photonics, solar cells, photo- and electrochromism, microelectronics, bio-oriented devices.<sup>165,166</sup> Therefore, a newly designed electrochemically assisted self-assembly method provides a fast and versatile way to generate highly ordered mesopore channels and creates a platform for the development of functionalized oriented films carrying functional groups such as ferrocene and cobaltocene with electron hopping between close redox sites as the charge transfer mechanism.<sup>165</sup>

Electro-responsive threadlike micelles were formed using new cationic gemini surfactants ( $\text{Fc}11\text{-n}11\text{-Fc}$ ) with redox-active ferrocenyl groups in the gemini alkyl chains and showed to form a class of highly viscous smart soft materials.<sup>167</sup> The new gelator, stigmasteryl glycinate ferrocenoylamide (SGF) utilizes plant sterols as raw materials and has multi-stimulus response performance with gelation behavior including lamellar aggregation pattern showing excellent responsiveness to redox stimuli.<sup>168</sup>

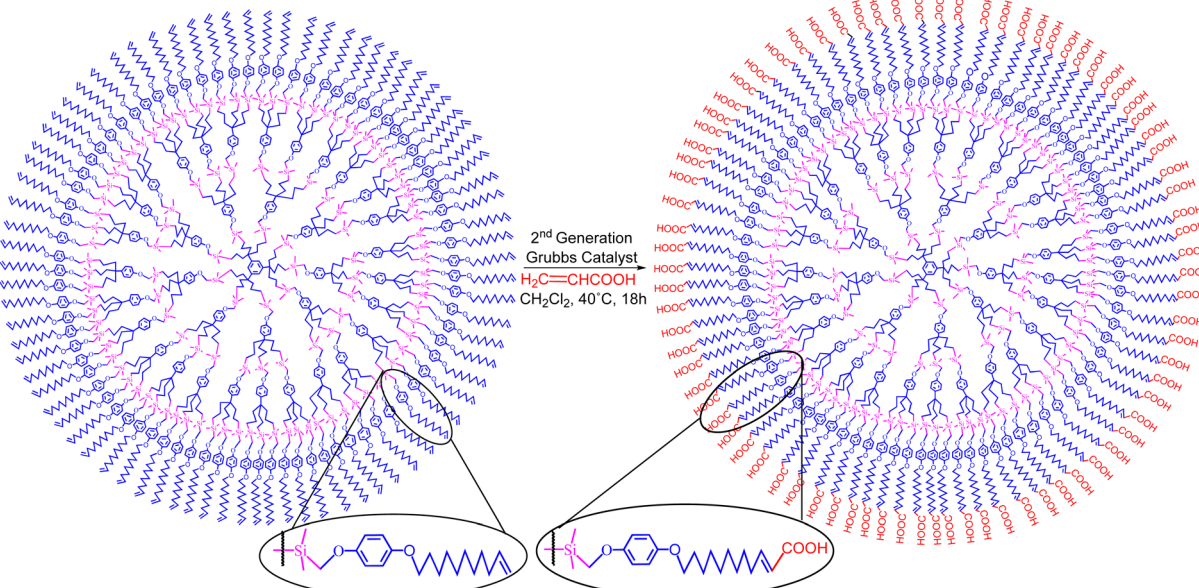
## VIII. Dendritic catalysis, unimolecular micellar effect, auto-catalysis, homeopathic catalysis, and nanozymes

In section VII, cross metathesis was shown to be useful as a dendrimer functionalization strategy. Other efficient dendrimer functionalization methods involved, for instance ETC reactions<sup>26</sup> using the  $\text{Fe}(\text{i})$  sandwich **1a** as initiator, as shown in Scheme 2. When dendrimers were decorated with 32 or 64  $\text{CH}_2\text{PPh}_2$  groups, ETC exchange of a carbonyl ligand of the well-known cluster  $[\text{Ru}_3(\text{CO})_{12}]$  by each of the dendritic phosphine using 1% mol equiv. of this initiator, **1a**, was very clean at ambient temperature as shown by  $^{31}\text{P}$  NMR and provided multi cluster-functionalized dendrimers.<sup>169,170</sup> A dendrimer with nona-peroxophospho-tungstate  $\{[\text{PO}_4\{\text{WO}(\text{O}_2)_2\}_4]^{3-}\}$  tri(hexyl) ammonium salts as termini synthesized by functionalization of the nona-allyl arene proved to be a mild, efficient and fully recyclable metallocendritic catalyst for the epoxidation of olefins by  $\text{H}_2\text{O}_2$  in water/ $\text{CDCl}_3$  and for the oxidation of thioanisole to sulfone.<sup>171</sup> In this latter case, as in many others in the literature for a variety of reactions,<sup>172</sup> the dendrimer acts as a support allowing catalyst recycling. Dendritic unimolecular micelles such as that synthesized according to Scheme 16 served as catalyst templates for various catalytic reactions in water or aqueous media including olefin metathesis reactions,<sup>172–174</sup> click chemistry,<sup>174–176</sup> carbon–carbon coupling of Miyaura–Suzuki or Sonogashira type<sup>177–179</sup> and redox reactions including nitrophenol reduction<sup>179–182</sup> by  $\text{NaBH}_4$ <sup>183</sup> or aerobic benzylic alcohol oxidation.<sup>184</sup> Click dendrimers were indeed major candidates for the mild stabilization of efficient gold and palladium nanocatalysts and nanosensors,<sup>185,186</sup> although efficient gold nanocatalysts<sup>185–187</sup> were also synthesized by simple  $\text{Au}(\text{iii})$





**Scheme 14** Single-pot  $\text{CpFe}^+$ -induced nona-allylation of mesitylene followed by olefin metathesis reaction of the 9 terminal double bonds catalyzed by the 2nd-generation Ru Grubbs catalyst: cyclophane cage synthesis (left) or cyclization of two tethers of each tripod along with functionalization of the 3rd one in the presence of acrylic acid or acrylate (right). Adapted with permission of ref. 140. Copyright 2008 American Chemical Society.



**Scheme 15** Selective functionalization of olefin-terminated dendrimers by cross metathesis. Reproduced with permission from ref. 157. Copyright 2008 American Chemical Society.

reduction with  $\text{NaBH}_4$ .<sup>188</sup> This dendrimer synthesis of Scheme 16 itself is autocatalytic,<sup>175</sup> since conducting the reaction in the presence of 1% of the final product more than doubled the reaction yield, and the conversion yield was already 46% after 1.5 h instead of 2% in absence of this addition. The reason of the autocatalysis is that the dendrimer served as a template for the substrates. These micellar-type reactions needed only a small amount (such as 0.1 mol%) of the dendritic micelle<sup>42</sup> (that was fully recyclable) and involved only a few ppm of nanocatalyst (and even less than 1 ppm for some Miyaura–Suzuki reactions). With triazolyl-ferrocene terminated click dendrimers, these reactions required, at ambient temperature, all the less ppm Pd catalyst as

the concentration was lower, which led to the concept of “homeopathic catalysis”. This phenomenon, known in de Vries’ work for Heck reactions at 130 °C,<sup>189</sup> was taken into account by tiny catalytic cluster loss from the mother nanoparticle that recombined all the less easily as the nanoparticle concentration was lower.<sup>190–192</sup>

The localization and shape of nanoparticles encapsulated in dendrimers also play key roles on their catalytic activity, depending on the reaction involved.<sup>193,194</sup> In most of these reactions, especially micellar ones, the dendrimer-nanocatalyst assembly behaves as an enzyme, *i.e.* it represents a nanozyme, a known biochemical concept.<sup>195,196</sup> For instance, with Cu(I)-tren-centered dendrimer terminated with 18 or 54 tri(ethyleneglycol)



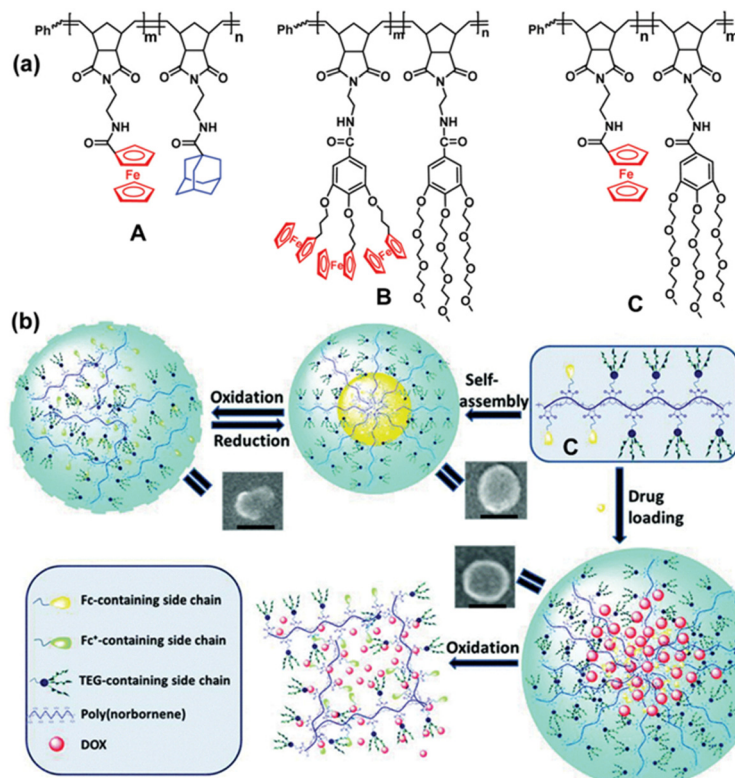
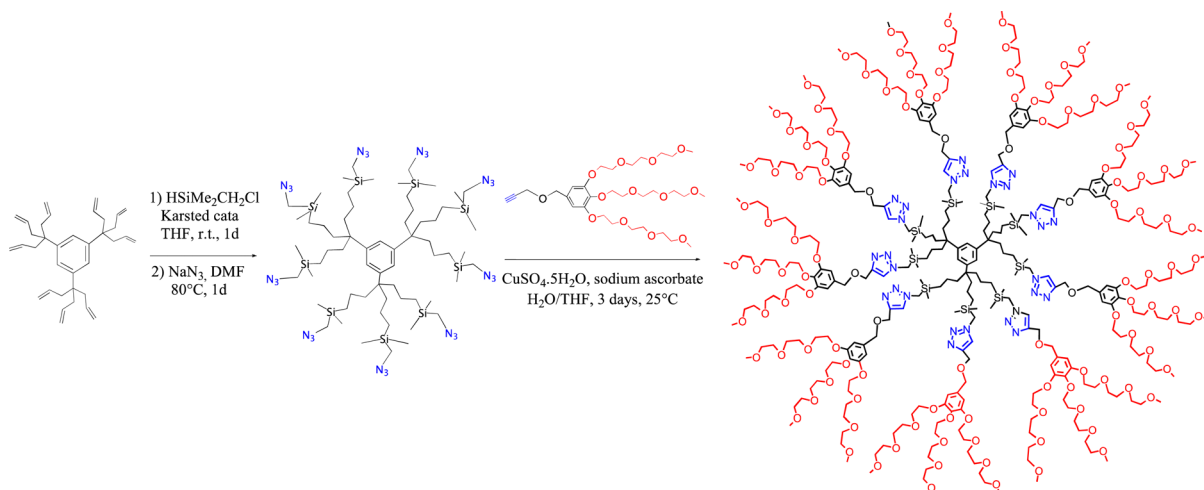


Fig. 22 (a) ROMP-synthesized metallocopolymers A, B and C containing ferrocenes. A forms an amphiphile upon  $\beta$ -cyclodextrin addition, and B and C are amphiphiles that self-assembles in redox-responsive micelle (b) Redox-controlled micelles of C for the encapsulation/release of drugs upon redox switch of the ferrocene units; SEM images are shown (scale bar: 100 nm). Reproduced with permission from ref. 163. Copyright 2019 Royal Society of Chemistry.



Scheme 16 Synthesis of a dendritic unimolecular micelle as template for multiple catalytic uses (molecular catalysis with Grubbs II catalyst, metal ion click catalysis with Cu(II), and nanoparticle catalysis).

branches, kinetic studies with phenyl acetylene and benzyl azide showed even faster reactions than with non-dendritic Cu(I)-(PhCH<sub>2</sub>)<sub>6</sub>tren, a trend similar to that known with enzymes.<sup>197</sup> Click-dendrimer-Pd nanoparticle assemblies also behaved as enzyme mimics in the colorimetric H<sub>2</sub>O<sub>2</sub> detection upon catalytic *o*-phenylene diamine oxidation.<sup>198</sup>

## IX. Hydrogen production

Hydrogen (H<sub>2</sub>) is crucial for sustainable energy of the future.<sup>199</sup> Therefore, the necessity of safe H<sub>2</sub> carriers to minimize risks and insure H<sub>2</sub> storage and transportation has undergone considerable research.<sup>200</sup> Boranes and related derivatives<sup>201</sup> are hydrogen rich, and their hydrolysis under ambient conditions,

providing H<sub>2</sub> in the presence of various transition metal-based nanocatalysts, has drawn the attention of chemists,<sup>201–203</sup> with particular emphasis first on NaBH<sub>4</sub>, then on ammonia–borane, NH<sub>3</sub>BH<sub>3</sub>.<sup>203</sup> If these two derivatives are the most investigated ones, research has been extended to others in the liquid phase such as hydrazine borane, silanes, formic acid and other hydrocarbons.<sup>203,204</sup> Our group has studied a variety of these hydrogen carriers essentially using, as nanocatalyst stabilizers, either click dendrimers<sup>205–208</sup> or MOFs of the ZIF-8 type,<sup>209–216</sup> because both of these families, beside their steric effects, contain nitrogen atoms that mildly stabilize nanoparticle catalysts for optimized reactions and provide synergy in catalysis. In these reactions, one hydrogen atoms of H<sub>2</sub> formed is provided by the hydrogen carrier, and the other from water, which is shown by labeling experiments.<sup>215</sup> Kinetic isotope effects and DFT calculations have provided evidence that water activation is the rate-determining step, facilitated by hydrogen bonding with the hydridic atom coming from the carrier at the nanocatalyst surface.<sup>195</sup> In the particular case of the nanocatalyzed hydrolysis of bis-boric acid, {B<sub>2</sub>(OH)<sub>4</sub>}, however, both hydrogen atoms of H<sub>2</sub> formed are coming from water, the side product being boric acid, B(OH)<sub>3</sub>.<sup>207,217</sup> The H<sub>2</sub> generation reaction rates can be switched on and off for instance by pH control,<sup>212,215,217</sup> or be boosted by visible-light irradiation, either upon including a semiconductor in the nanocatalyst composite (Mott–Schottky junction at the metal–semiconductor interface),<sup>211</sup> or more efficiently utilizing the Ag or Au plasmon<sup>207–209,215–219</sup> or a combination of both the semiconductor and plasmonic effects.<sup>211</sup> The studies of these nanocatalysts bring about considerable knowledge on how the key nanocatalyst hydride are formed and how they reductively eliminate to give H<sub>2</sub>. In particular, the introduction of negative charges onto the nanocatalyst by anion coordination or plasmonic hot electron transfer has been shown to boost H<sub>2</sub> formation during these reactions, which also is of interest for other energy-providing nanocatalyzed or electrocatalyzed reactions. This detailed mechanistic information disclosed here, confirmed by DFT studies, is also useful for the design of energy-related catalytic devices.<sup>220–223</sup>

## X. Conclusion and outlook

The simplest chemical events, electron transfer and proton transfer, have been utilized with late transition metal sandwiches whose robustness was eventually reinforced by sandwich ring permethylation. The considerable acidity increase of these juxtaglycine methyl or alkyl groups compared to isostructural neutral compounds has allowed us to establish in the late 1970s a novel and powerful method of multiple C–C bond formation that led to the formation of molecular stars and dendrimers. It is also the choice of such robust cationic 18-electron complexes that afforded easily synthesizing very electron-rich 19-electron complexes, yet at redox potential far less negative than isolobal ferrocene anion that cannot be synthesized. The designed 19-electron and 17-electron iron

complexes, besides original electronic properties including mixed and average valencies and application to battery materials, are very useful stoichiometric redox reagents and also possess redox catalyst and electrocatalyst properties allowing many redox transformations of a variety of substrates.

The resulting dendrimer structure with 1 → 3 branching led us to the design of the first click metallodendrimers, *i.e.* with metals either attached to the termini of the dendritic tethers or as nanoparticles coordinated to the triazole link. This specifically mild triazole coordination to nanoparticles rendered these nanocatalysts extremely efficient for a broad range of key reactions including C–C or C–N bond formation in substrates as well as fast and efficient H<sub>2</sub> generation from hydrogen-rich precursors, sometimes accelerated by visible light illumination, for instance when the alloy contains a plasmonic metal besides the substrate-activating metal.

Focusing on electron and proton transfer processes obviously involved a biological context and applications, as already noticed at an early time by the easy generation and demonstration of great reactivity of superoxide radical anion and the total inhibition of its reactions in the model system. Redox catalysis of reduction of nitrogen oxide and other nitro derivatives catalyzed by Fe(I) or nanoparticles is a method of choice of their destruction from the environment. Olefin metathesis reactions are a useful complement to the dendritic structure in molecular engineering towards both redox sensing and drug delivery, for which the redox aspect of the metal sandwich compounds plays an essential part. The supramolecular aspect of these ensembles plays a key role in their properties and functions, as exemplified by the *in vitro* toxicity of dendritic structures in docetaxel delivery against prostate cancer and theranostic application of fluorescent vesosomes produced upon metallodendrimers assembly.

In the future, such sophistication of molecular and inorganic devices and their interplay should be essential, in particular in the design of both optimized nanocatalysts for energy conversion and “magic bullets” for drug delivery.

## Conflicts of interest

There are no conflicts to declare.

## Acknowledgements

Contributions and enlightening and enthusiastic discussions with the numerous colleagues and students cited in the references, and financial support from the University of Bordeaux, the Centre National de la Recherche Scientifique (CNRS), L’Oréal Recherche, the Institut Universitaire de France, the Agence National pour la Recherche (ANR), the Nanosolution European FP7 program, the China Scholarship Council (CSC) and 111 Project of China are gratefully acknowledged.

## References

- 1 T. J. Kealy and P. L. Pauson, *Nature*, 1951, **168**, 1039–1040.
- 2 I. Langmuir, *Science*, 1921, **54**, 59–67.



3 R. B. Woodward, M. Rosenblum and M. C. Whiting, *J. Am. Chem. Soc.*, 1952, **74**, 3458–3459.

4 G. Wilkinson, *J. Organomet. Chem.*, 1975, **100**, 273–278.

5 M. L. H. Green and G. Parkin, *J. Chem. Ed.*, 2014, **91**, 807–816.

6 P. Stepnicka, *Dalton Trans.*, 2022, **51**, 8085–8102.

7 M. C. Baird, *J. Organomet. Chem.*, 2014, **751**, 50–54.

8 A. N. Nesmeyanov, N. A. Volkenau and I. N. Bolesova, *Tetrahedron Lett.*, 1963, **4**, 1725–1729.

9 D. Astruc, J.-R. Hamon, G. Althoff, E. Román, P. Batail, P. Michaud, J.-P. Mariot, F. Varret and D. Cozak, *J. Am. Chem. Soc.*, 1979, **101**, 5445–5447.

10 J.-R. Hamon, D. Astruc and P. Michaud, *J. Am. Chem. Soc.*, 1981, **103**, 758–766.

11 M. V. Rajasekharan, S. Gieyzynski, J. H. Ammeter, N. Oswald, J.-R. Hamon, P. Michaud and D. Astruc, *J. Am. Chem. Soc.*, 1982, **104**, 2400–2407.

12 D. Astruc, *Acc. Chem. Res.*, 1986, **19**, 377–383.

13 D. Astruc, E. Román, J.-R. Hamon and P. Batail, *J. Am. Chem. Soc.*, 1979, **101**, 2240–2242.

14 D. Astruc, J.-R. Hamon, E. Román and P. Michaud, *J. Am. Chem. Soc.*, 1981, **103**, 7502–7514.

15 J.-R. Hamon, D. Astruc, E. Román, P. Batail and J. J. Mayerle, *J. Am. Chem. Soc.*, 1981, **103**, 2431–2433.

16 J.-R. Hamon and D. Astruc, *J. Am. Chem. Soc.*, 1983, **105**, 5951–5953.

17 T. Finkel and N. J. Holbrook, *Nature*, 2000, **408**, 239–247.

18 A. Loupy, B. Tchoubar and D. Astruc, *Chem. Rev.*, 1992, **92**, 1141–1165.

19 C. Bossard, S. Rigaut, D. Astruc, M.-H. Delville, G. Félix, A. Février-Bouvier, J. Amiell, S. Flandrois and P. Delhaës, *J. Chem. Soc., Chem. Commun.*, 1993, 333–334.

20 D. Méry, J. Ruiz and D. Astruc, *J. Am. Chem. Soc.*, 2006, **128**, 5602–5603.

21 F. Fu, A. Dedieu, W. Wang, T. Chen, Y. Song, E. Fouquet, J.-R. Hamon, M. Zhu and D. Astruc, *Chem. Commun.*, 2019, 55, 10277–10280.

22 S. Rigaut, M.-H. Delville and D. Astruc, *J. Am. Chem. Soc.*, 1997, **119**, 11132–11133.

23 S. Rigaut, M.-H. Delville, J. Losada and D. Astruc, *Inorg. Chim. Acta*, 2002, **334**, 225–242.

24 J. Ruiz, M. Lacoste and D. Astruc, *J. Am. Chem. Soc.*, 1990, **112**, 5471–5483.

25 D. S. Brown, M.-H. Delville, R. Boese, K. P. C. Vollhardt and D. Astruc, *Angew. Chem., Int. Ed. Engl.*, 1994, **33**, 661–663.

26 D. Astruc, *Angew. Chem., Int. Ed. Engl.*, 1988, **27**, 643–660.

27 H. Taube, *Chem. Rev.*, 1952, **50**, 69–126.

28 J. Ruiz and D. Astruc, *C. R. Séances Acad. Sci., Ser. C*, 1998, 21–27.

29 I. Noviandri, K. N. Brown, D. S. Fleming, P. T. Gulyas, P. A. Lay, A. F. Masters and L. Phillips, *J. Phys. Chem. B*, 1999, **103**, 6713–6722.

30 C. A. P. Goodwin, M. J. Giansiracusa, S. M. Greer, H. M. Nicholas, P. Evans, M. Vonci, S. Hill, N. F. Chilton and D. P. Mills, *Nat. Chem.*, 2021, **13**, 243–248.

31 H. A. Trujillo, C. Casado, J. Ruiz and D. Astruc, *J. Am. Chem. Soc.*, 1999, **121**, 5674–5686.

32 J. Ruiz, F. Ogliaro, J.-Y. Saillard, J.-F. Halet, F. Varret and D. Astruc, *J. Am. Chem. Soc.*, 1998, **120**, 11693–11705.

33 N. G. Connally and W. E. Geiger, *Chem. Rev.*, 1996, **96**, 877–910.

34 H. Nishihara, *Adv. Inorg. Chem.*, 2002, **53**, 41–86.

35 D. Astruc, *Electron Transfer and Radical Processes, Transition-Metal Chemistry. Part I: Theories, Techniques, Electronic Structures and Molecular Electronics. Part II: Mechanisms, Catalysis and Applications to Synthesis*, VCH, New York, 1995, p. 630, ISBN 1-56081-566-3; foreword: Henry Taube.

36 M.-H. Desbois and D. Astruc, *New J. Chem.*, 1989, **13**, 595–600.

37 D. Astruc, *Acc. Chem. Res.*, 1991, **24**, 36–42.

38 J. L. Hérisson and Y. Chauvin, *Makromol. Chem.*, 1971, **141**, 161–176.

39 T. J. Katz, *Adv. Organomet. Chem.*, 1978, **16**, 283–317.

40 D. Astruc, *Organometallic Chemistry and Catalysis*, Springer, Berlin, 2007, p. 608, ISBN 978-3-540-46128-9. French edition: Chimie organométallique et catalyse. EDP Sciences, Les Ullis, 2013.

41 D. A. Tomalia, A. M. Naylor and W. A. Goddard, *Angew. Chem., Int. Ed. Engl.*, 1990, **29**, 138–175.

42 G. R. Newkome, E. F. He and C. N. Moorefield, *Chem. Rev.*, 1999, **99**, 1689–1746.

43 A. M. Caminade and J. P. Majoral, in *Dendrimers*, ed. F. Vögtle, *Top. Curr. Chem.*, 1998, vol. 197, pp. 79–124.

44 F. Moulines, L. Djakovitch, R. Boese, B. Gloaguen, W. Thiel, J.-L. Fillaut, M.-H. Delville and D. Astruc, *Angew. Chem., Int. Ed. Engl.*, 1993, **32**, 1075–1077.

45 F. Moulines, B. Gloaguen and D. Astruc, *Angew. Chem., Int. Ed. Engl.*, 1992, **31**, 458–460.

46 J.-R. Hamon, J.-Y. Saillard, A. Le Beuze, M. J. McGlinchey and D. Astruc, *J. Am. Chem. Soc.*, 1982, **104**, 7549–7555.

47 F. Moulines and D. Astruc, *Angew. Chem., Int. Ed. Engl.*, 1988, **27**, 1347–1349.

48 J. Ruiz, G. Lafuente, S. Marcen, C. Ornelas, S. Lazare, E. Cloutet, J.-C. Blais and D. Astruc, *J. Am. Chem. Soc.*, 2003, **125**, 7250–7257.

49 V. Sartor, L. Djakovitch, J.-L. Fillaut, F. Moulines, F. Neveu, V. Marvaud, J. Guittard, J.-C. Blais and D. Astruc, *J. Am. Chem. Soc.*, 1999, **121**, 2929–2930.

50 G. R. Newkome and C. Shreiner, *Chem. Rev.*, 2010, **110**, 6338–6442.

51 P.-G. De Gennes and H. Hervet, *J. Phys. Lett.*, 1983, **44**, L351–L360.

52 V. Martinez, J.-C. Blais and D. Astruc, *Angew. Chem., Int. Ed.*, 2003, **42**, 4366–4369.

53 D. Catheline and D. Astruc, *J. Organomet. Chem.*, 1984, **272**, 417–426.

54 D. Astruc, *New J. Chem.*, 1992, **16**, 305–328.

55 B. Gloaguen and D. Astruc, *J. Am. Chem. Soc.*, 1990, **112**, 4607–4609.

56 D. Buchholz, B. Gloaguen, J.-L. Fillaut, M. Cotrait and D. Astruc, *Chem. – Eur. J.*, 1995, **1**, 374–381.

57 D. Buchholz and D. Astruc, *Angew. Chem., Int. Ed. Engl.*, 1994, **33**, 1637–1639.

58 D. Astruc, *Acc. Chem. Res.*, 2000, **33**, 287–298.

59 M.-H. Desbois and D. Astruc, *Angew. Chem., Int. Ed. Engl.*, 1989, **28**, 460–461.

60 M.-H. Delville, S. Mross, D. Astruc, J. Linares, F. Varret, H. Rabaa, A. Le Beuze, J.-Y. Saillard, R. D. Culp, D. A. Atwood and A. H. Cowley, *J. Am. Chem. Soc.*, 1996, **118**, 4133–4147.

61 D. O. Cowan, C. LeVanda, J. Park and F. Kaufmann, *Acc. Chem. Res.*, 1973, **6**, 1–7.

62 G. C. Allen and N. S. Hush, *Prog. Inorg. Chem.*, 1967, **8**, 357–389.

63 M. B. Robin and P. Day, *Adv. Inorg. Chem. Radiochem.*, 1968, **10**, 247–422.

64 C. Creuz and H. Taube, *J. Am. Chem. Soc.*, 1969, **91**, 3988–3989.

65 D. Astruc, *Acc. Chem. Res.*, 1997, **30**, 383–391.

66 D. Astruc, *Chem. – Eur. J.*, 2021, **27**, 16291–16308.

67 M.-H. Desbois, D. Astruc, J. Guillen, J.-P. Mariot and F. Varret, *J. Am. Chem. Soc.*, 1985, **107**, 5280–5282.

68 M.-H. Desbois, D. Astruc, J. Guillen, F. Varret, A. X. Trautwein and G. Villeneuve, *J. Am. Chem. Soc.*, 1989, **111**, 5800–5809.

69 M.-H. Delville-Desbois, M. Lacoste and D. Astruc, *J. Am. Chem. Soc.*, 1992, **114**, 8310–8311.

70 M. Lacoste, F. Varret, L. Toupet and D. Astruc, *J. Am. Chem. Soc.*, 1987, **109**, 6504–6506.

71 M. Lacoste, H. Rabaa, D. Astruc, N. Ardoin, F. Varret, J.-Y. Saillard and A. Le Beuze, *J. Am. Chem. Soc.*, 1990, **112**, 9548–9557.

72 A. K. Diallo, J.-C. Daran, F. Varret, J. Ruiz and D. Astruc, *Angew. Chem., Int. Ed.*, 2009, **48**, 3141–3145.

73 A. K. Diallo, C. Absalon, J. Ruiz and D. Astruc, *J. Am. Chem. Soc.*, 2011, **133**, 629–641.

74 D. Astruc, *Nat. Chem.*, 2012, **4**, 255–267.

75 F. Paul and C. Lapinte, *Coord. Chem. Rev.*, 1998, **178–180**, 431–509.

76 Y. Wang, L. Salmon, J. Ruiz and D. Astruc, *Nat. Commun.*, 2014, **5**, 3489.

77 R. L. N. Hailes, A. M. Oliver, J. Gwyther, G. R. Whytell and I. Manners, *Chem. Soc. Rev.*, 2016, **45**, 5358–5407.

78 C. Deraedt, A. Rapakousiou, Y. Wang, L. Salmon, M. Bousquet and D. Astruc, *Angew. Chem., Int. Ed.*, 2014, **53**, 8445–8449.

79 H. Gu, R. Ciganda, P. Castel, S. Moya, R. Hernandez, J. Ruiz and D. Astruc, *Angew. Chem., Int. Ed.*, 2018, **57**, 2204–2208.

80 P. Roland, E. Schoeter, O. Nolte, G. R. Newkome, M. D. Hager and U. S. Schubert, *Prog. Mater. Sci.*, 2022, **125**, 101474.

81 K. S. Park, S. B. Schougaard and J. B. Goodenough, *Adv. Mater.*, 2007, **19**, 848–851.

82 S. M. Beladi-Mousavi, S. Sadaf, L. Walder, M. Gallei, C. Rüttiger, S. Eigler and C. E. Halbig, *Adv. Energy Mater.*, 2016, **6**, 1600108.

83 B. Hwang, M.-S. Park and K. Kim, *ChemSusChem*, 2015, **8**, 310–314.



84 S. M. Beladi-Messavi, S. Sadaf, A. K. Hennecke, J. Klein, A. M. Mahmood, C. Ruttiger, M. Gallei, F. Fu, E. Fouquet, J. Ruiz, D. Astruc and L. Walder, *Angew. Chem., Int. Ed.*, 2021, **60**, 13554–13558.

85 X. S. M. Beladi-Messavi and L. Walder, *Polymer*, 2022, **245**, 124658.

86 D. Y. Kuo, P. S. Price, S. Raugei and B. M. Cossairt, *J. Phys. Chem. C*, 2022, **126**, 13994–14002.

87 C. Ornelas, J. Ruiz, C. Belin and D. Astruc, *J. Am. Chem. Soc.*, 2009, **131**, 590–601.

88 D. Astruc, C. Ornelas and J. Ruiz, *Chem. – Eur. J.*, 2009, **15**, 8936–8944.

89 C. Ornelas, J. Ruiz and D. Astruc, *Organometallics*, 2009, **28**, 2716–2723.

90 R. Djeda, C. Ornelas, J. Ruiz and D. Astruc, *Inorg. Chem.*, 2010, **49**, 6085–6101.

91 J.-M. Lehn, *Angew. Chem., Int. Ed. Engl.*, 1990, **29**, 1304–1319.

92 P. D. Beer and P. A. Gale, *Angew. Chem., Int. Ed.*, 2001, **40**, 486–516.

93 R. L. Sun, L. Wang, H. J. Yu, Zain-ul-Abdin, Y. S. Chen, J. Huang and R. B. Tong, *Organometallics*, 2014, **33**, 4560–4573.

94 C. X. Zhu, D. Liu, Y. Y. Li, S. Ma, M. Wang and T. Y. Yu, *Biosens. Bioelectron.*, 2021, **174**, 112654.

95 H. Y. Li, Q. Li, S. X. Zhao, X. M. Wang and F. Li, *J. Agric. Food Chem.*, 2022, **70**, 680–686.

96 X. Y. Hua, H. L. Wang, Y. Q. Wen, X. J. Zhang and L. Su, *Sens. Actuators, B*, 2022, **372**, 132610.

97 S. N. Feng, Y. Xue, J. S. Huang and X. R. Yang, *Anal. Chem.*, 2022, **94**, 16945–16952.

98 R. J. Zeng, J. H. Xu, T. K. Liang, M. J. Li and D. P. Tang, *ACS Sens.*, 2023, **8**, 317–325.

99 M. Y. Wang, W. J. Jing, L. J. Wang, L. P. Jia, R. N. Ma, W. Zhang, L. Shang, X. J. Li, Q. W. Xu and H. S. Wang, *Biosens. Bioelectron.*, 2023, **226**, 115116.

100 C. Valério, J.-L. Fillaut, J. Ruiz, J. Guittard, J.-C. Blais and D. Astruc, *J. Am. Chem. Soc.*, 1997, **119**, 2588–2589.

101 S. Nlate, J. Ruiz, J.-C. Blais and D. Astruc, *Chem. Commun.*, 2000, 417–418.

102 M.-C. Daniel, J. Ruiz, J.-C. Blais, N. Daro and D. Astruc, *Chem. – Eur. J.*, 2003, **9**, 4371–4379.

103 S. R. Miller, D. A. Gustowski, Z.-H. Chen, G. W. Gokel, L. Echegoyen and A. E. Kaifer, *Anal. Chem.*, 1988, **60**, 2021–20924.

104 C. M. Casado, I. Cuadrado, M. Moran, B. Alonso, B. Garcia, B. Gonzales and J. Losada, *Coord. Chem. Rev.*, 1999, **185–186**, 53–79.

105 C. M. Cardona, S. Mendoza and A. E. Kaifer, *Chem. Soc. Rev.*, 2000, **29**, 37–42.

106 C. Valério, E. Alonso, J. Ruiz, J.-C. Blais and D. Astruc, *Angew. Chem., Int. Ed.*, 1999, **38**, 1747–1751.

107 M. Yamada and H. Nishihara, *C. R. Chimie*, 2001, **6**, 919–934.

108 A. Labande, J. Ruiz and D. Astruc, *J. Am. Chem. Soc.*, 2002, **124**, 1782–1789.

109 M.-C. Daniel, J. Ruiz, S. Nlate, J.-C. Blais and D. Astruc, *J. Am. Chem. Soc.*, 2003, **125**, 2617–2628.

110 M.-C. Daniel, J. Ruiz and D. Astruc, *J. Am. Chem. Soc.*, 2003, **125**, 1150–1151.

111 H. Gu, A. Rapakousiou, P. Castel, N. Guidolin, N. Pinaud, J. Ruiz and D. Astruc, *Organometallics*, 2014, **33**, 4323–4335.

112 H. C. Kolb, M. G. Finn and K. B. Sharpless, *Angew. Chem., Int. Ed.*, 2001, **40**, 2004–2021.

113 M. Meldal and C. W. Tornøe, *Chem. Rev.*, 2008, **108**, 2952–3015.

114 C. R. Bercer, R. Hoogenboom and U. S. Schubert, *Angew. Chem., Int. Ed.*, 2009, **48**, 4900–4908.

115 C. Ornelas, J. Ruiz, E. Cloutet, S. Alves and D. Astruc, *Angew. Chem., Int. Ed.*, 2007, **46**, 872–877.

116 C. Ornelas, L. Salmon, J. Ruiz and D. Astruc, *Chem. – Eur. J.*, 2008, **14**, 50–64.

117 R. Djeda, A. Rapakousiou, L. Liang, N. Guidolin, J. Ruiz and D. Astruc, *Angew. Chem., Int. Ed.*, 2010, **49**, 8152–8156.

118 S. Badèche, J.-C. Daran, J. Ruiz and D. Astruc, *Inorg. Chem.*, 2008, **47**, 4903–4908.

119 D. Astruc, C. Ornelas and J. Ruiz, *J. Inorg. Organomet. Polym. Mater.*, 2008, **18**, 4–17.

120 E. Boisselier, L. Salmon, J. Ruiz and D. Astruc, *Chem. Commun.*, 2008, 5788–5790.

121 C. Ornelas, L. Salmon, J. Ruiz and D. Astruc, *Chem. Commun.*, 2007, 4946–4948.

122 J. Camponovo, J. Ruiz, E. Cloutet and D. Astruc, *Chem. – Eur. J.*, 2009, **15**, 2990–3002.

123 H.-W. Marx, F. Moulines, T. Wagner and D. Astruc, *Angew. Chem., Int. Ed. Engl.*, 1996, **35**, 1701–1704.

124 A. N. Nesmeyanov, L. G. Bogomolova and V. Viltcheskaya, *US Pat.*, 119 356, 1971.

125 V. J. Fiorina, R. J. Dubois and S. Brynes, *J. Med. Chem.*, 1978, **21**, 393–395.

126 C. Biot, G. Glorian, L. A. Maciejewski and J. Brocard, *J. Med. Chem.*, 1997, **40**, 3715–3718.

127 M. Patra and G. Gasser, *Nat. Rev. Chem.*, 2017, **1**, 0066.

128 C. Ornelas, *New J. Chem.*, 2011, **35**, 973–1985.

129 G. Jaouen, A. Vessieres and S. Top, *Chem. Soc. Rev.*, 2015, **44**, 8802–8817.

130 C. Fang, Z. Deng, G. D. Cao, Q. Chu, Y. L. Wu, X. Li, X. S. Peng and G. R. Han, *Adv. Funct. Mater.*, 2020, **30**, 1910085.

131 L. L. Zhang, R. Abdullah, X. X. Hu, H. R. Bai, H. H. Fan, L. He, H. Liang, J. M. Zou, Y. L. Liu and Y. Sun, *J. Am. Chem. Soc.*, 2019, **141**, 4282–4290.

132 X. Liu, Z. F. Wu, C. J. Guo, H. M. Guo, Y. G. Su, Q. Chen, C. G. Sun, Q. M. Liu, D. Q. Chen and H. J. Mu, *Drug Delivery*, 2022, **29**, 138–148.

133 W. J. Wang, Y. Y. Ling, Y. M. Zhong, Z. Y. Li, C. P. Tan and Z. W. Mao, *Angew. Chem., Int. Ed.*, 2022, **61**, e202115247.

134 D. Astruc, *C. R. Séances Acad. Sci., Ser. B*, 1996, **322**, 757–766.

135 C. C. Lee, J. A. MacKay, J. M. J. Fréchet and F. C. Szoka, *Nat. Biotechnol.*, 2005, **23**, 1517–1526.

136 J. Khandare, M. Calderon, N. M. Dapia and R. Haag, *Chem. Soc. Rev.*, 2012, **41**, 2824–2848.

137 R. M. Kannan, E. Nance, S. Kannan and D. A. Tomalia, *J. Intern. Med.*, 2014, **276**, 579–617.

138 A.-M. Caminade and C.-O. Turrin, *J. Mater. Chem. B*, 2014, **2**, 4055–4066.

139 E. Boisselier, A. K. Diallo, L. Salmon, C. Ornelas, J. Ruiz and D. Astruc, *J. Am. Chem. Soc.*, 2010, **132**, 2729–2742.

140 E. Boisselier, L. Liang, M. Dalko-Csiba, J. Ruiz and D. Astruc, *Chem. – Eur. J.*, 2010, **16**, 6056–6068.

141 D. Guénard, F. Guérat-Voegelein and P. Pottier, *Acc. Chem. Res.*, 1993, **26**, 160–167.

142 P. Zhao and D. Astruc, *ChemMedChem*, 2012, **7**, 952–972.

143 A. François, A. Laroche, N. Pinaud, L. Salmon, J. Ruiz, J. Robert and D. Astruc, *ChemMedChem*, 2011, **6**, 2003–2008.

144 T. Förster and K. Kasper, *Z. Phys. Chem.*, 1954, **1**, 275–277.

145 J. D. Luo, Z. L. Xie, J. W. Y. Lam, L. Cheng, H. Y. Chen, C. F. Qiu, H. S. Kwok, X. W. Zhan, Y. Q. Liu, D. B. Zhu and B. Z. Tang, *Chem. Commun.*, 2001, 1740–1741.

146 J. Mei, N. L. C. Leung, R. T. K. Kwok, J. W. Y. Lam and B. Z. Tang, *Chem. Rev.*, 2015, **115**, 11718–11940.

147 Y. Wang, H. Li, D. Wang and B. Z. Tang, *Adv. Funct. Mater.*, 2021, **31**, 2006952.

148 X. Zhou, W. Luo, H. Nie, L. Xu, R. Hu, Z. Zhao, A. Qin and B. Z. Tang, *J. Mater. Chem. C*, 2017, **5**, 4775–4779.

149 M. Studzian, L. Pulaski, D. A. Tomalia and B. Klajnert-Maculewicz, *J. Phys. Chem. C*, 2019, **123**, 18007–18016.

150 D. A. Tomalia, B. Klajnert-Maculewicz, K. A. M. Johnson, H. F. Brinkman, A. Janaszewska and D. M. Hedstrand, *Prog. Polym. Sci.*, 2019, **90**, 35–117.

151 G. Perli, Qi Wang, C. B. Braga, D. L. Bertuzzi, L. A. Fontana, M. C. P. Soares, J. Ruiz, J. D. Megiatto, D. Astruc and C. Ornelas, *J. Am. Chem. Soc.*, 2021, **143**, 12948–12954.

152 Y. Chauvin, *Angew. Chem., Int. Ed.*, 2006, **45**, 3740–3747.

153 R. R. Schrock, *Acc. Chem. Res.*, 1990, **23**, 158–165.

154 C. W. Bielawski and R. H. Grubbs, *Prog. Polym. Sci.*, 2007, **32**, 1–29.

155 S. Gatard, S. Nlate, E. Cloutet, G. Bravic, J.-C. Blais and D. Astruc, *Angew. Chem., Int. Ed.*, 2003, **42**, 452–456.

156 C. Ornelas, D. Méry, J. Ruiz, J.-C. Blais, E. Cloutet and D. Astruc, *Angew. Chem., Int. Ed.*, 2005, **44**, 7399–7404.

157 C. Ornelas, D. Méry, E. Cloutet, J. Ruiz and D. Astruc, *J. Am. Chem. Soc.*, 2008, **130**, 1495–1506.

158 N. Falcone and H. B. Kratz, *Chem. – Eur. J.*, 2018, **54**, 14316–14328.

159 M. F. Ni, N. Zhang, W. Xia, X. Wu, C. H. Yao, X. Liu, X. Y. Hu, C. Lin and L. Y. Wang, *J. Am. Chem. Soc.*, 2016, **138**, 6643–6649.



160 M. Fadeev, Y. Ouyang, G. Davidson-Rosenfeld and I. Wilner, *J. Electroanal. Chem.*, 2021, **904**, 115926.

161 H. Gu, S. Mu, G. Qiu, X. Liu, L. Zhang, Y. Yuan and D. Astruc, *Coord. Chem. Rev.*, 2018, **364**, 51–85.

162 H. B. Gu, R. Ciganda, P. Castel, A. Vax, D. Gregurec, J. Irigoyen, S. Moya, L. Salmon, P. X. Zhao, J. Ruiz, R. Hernandez and D. Astruc, *Chem. - Eur. J.*, 2015, **21**, 18177–18186.

163 G. R. Qiu, X. Liu, B. R. Wang, H. B. Gu and W. X. Wang, *Polym. Chem.*, 2019, **10**, 2527–2539.

164 X. Liu, A. Rapakousiou, C. Deraedt, R. Ciganda, Y. Wang, J. Ruiz and D. Astruc, *Chem. Commun.*, 2020, **56**, 11374–11385.

165 A. Walcarus, *Acc. Chem. Res.*, 2021, **54**, 3563–3575.

166 L. Liang, F. Qin, S. Wang, J. Wu, R. Li, Z. Wang, M. Ren, D. Liu, D. Wang and D. Astruc, *Coord. Chem. Rev.*, 2023, **478**, 214998.

167 J. Sugai, N. Saito, Y. Takahashi and Y. Kondo, *Colloids Surf.*, 2019, **572**, 197–202.

168 J. C. Wang, M. Chen, H. T. Zhao, H. Zhang, H. Zhang and X. Yang, *Colloids Surf.*, 2020, **39**, 100321.

169 E. Alonso and D. Astruc, *J. Am. Chem. Soc.*, 2000, **122**, 3222–3223.

170 D. Astruc, K. Heuze, S. Gatard, D. Méry, S. Nlate and L. Plault, *Adv. Synth. Catal.*, 2005, **347**, 329–338.

171 L. Plault, A. Hauseler, S. Nlate, D. Astruc, S. Gatard and R. Neumann, *Angew. Chem., Int. Ed.*, 2004, **43**, 2924–2928.

172 D. Astruc, E. Boisselier and C. Ornelas, *Chem. Rev.*, 2010, **110**, 1857–1959.

173 A. Diallo, E. Boisselier and D. Astruc, *Chem. - Eur. J.*, 2010, **16**, 11832–11835.

174 D. Astruc, L. Liang, A. Rapakousiou and J. Ruiz, *Acc. Chem. Res.*, 2012, **45**, 630–640.

175 C. Deraedt, N. Pinaud and D. Astruc, *J. Am. Chem. Soc.*, 2014, **136**, 12092–12098.

176 C. Wang, D. Wang, S. Yu, T. Cornilleau, J. Ruiz, L. Salmon and D. Astruc, *ACS Catal.*, 2016, **6**, 5424–5431.

177 F. Liu, X. Liu, D. Astruc and H. Gu, *J. Colloid Interface Sci.*, 2019, **533**, 161–170.

178 W. Wang, E. S. Chamkina, E. G. Cal, D. Di Silvio, M. Martínez Moro, S. Moya, J.-R. Hamon, D. Astruc and Z. B. Shifrina, *Dalton Trans.*, 2021, **50**, 11852–11860.

179 C. Deraedt, L. Salmon and D. Astruc, *Adv. Synth. Catal.*, 2014, **356**, 2525–2538.

180 D. Wang, C. Deraedt, L. Salmon, C. Labrugère, L. Etienne, J. Ruiz and D. Astruc, *Chem. - Eur. J.*, 2015, **21**, 1508–1519.

181 C. Deraedt, L. Salmon and D. Astruc, *Adv. Synth. Catal.*, 2014, **356**, 2525–2538.

182 C. Wang, R. Ciganda, L. Salmon, D. Gregurec, J. Irigoyen, S. Moya, J. Ruiz and D. Astruc, *Angew. Chem., Int. Ed.*, 2016, **55**, 3091–3095.

183 P. Michaud, D. Astruc and J. H. Ammeter, *J. Am. Chem. Soc.*, 1982, **104**, 3755–3757.

184 D. Wang, C. Deraedt, L. Salmon, C. Labrugère, L. Etienne, J. Ruiz and D. Astruc, *Chem. - Eur. J.*, 2015, **21**, 6501–6510.

185 M.-C. Daniel and D. Astruc, *Chem. Rev.*, 2004, **104**, 293–346.

186 D. Astruc, F. Lu and J. Ruiz, *Angew. Chem., Int. Ed.*, 2005, **44**, 7852–7872.

187 N. Li, P. Zhao and D. Astruc, *Angew. Chem., Int. Ed.*, 2014, **53**, 1756–1789.

188 C. Deraedt, L. Salmon, S. Gatard, R. Ciganda, R. Hernandez, J. Ruiz and D. Astruc, *Chem. Commun.*, 2014, **50**, 14194–14196.

189 J. G. A. de Vries, *Dalton Trans.*, 2006, 421–429.

190 A. K. Diallo, C. Ornelas, L. Salmon, J. Ruiz and D. Astruc, *Angew. Chem., Int. Ed.*, 2007, **46**, 8644–8648.

191 D. Astruc, *Tetrahedron Asym.*, 2010, **21**, 1041–1054.

192 C. Deraedt and D. Astruc, *Acc. Chem. Res.*, 2014, **47**, 494–503.

193 X. Liu, D. Gregurec, J. Irigoyen, A. Martinez, S. Moya, R. Ciganda, P. Hermange, J. Ruiz and D. Astruc, *Nat. Commun.*, 2016, **7**, 13152.

194 A. Rapakousiou, C. Deraedt, H. Gu, L. Salmon, C. Belin, J. Ruiz and D. Astruc, *J. Am. Chem. Soc.*, 2014, **136**, 13995–13998.

195 H. Wei and E. Wang, *Chem. Soc. Rev.*, 2013, **42**, 6060.

196 Y. Huang, J. Ren and X. Qu, *Chem. Rev.*, 2019, **119**, 4357–4412.

197 L. Liang, J. Ruiz and D. Astruc, *Adv. Synth. Catal.*, 2011, **353**, 3434–3450.

198 Y. Liu, R. Pereira Lopes, T. Lüdtke, D. Di Silvio, S. Moya, J.-R. Hamon and D. Astruc, *Inorg. Chem. Front.*, 2021, **8**, 3301–3307.

199 M. L. Yue, H. Lambert, E. Pahon, R. Roche, S. Jemei and D. Hissel, *Renewable Sustainable Energy Rev.*, 2021, **146**, 111180.

200 T. He, P. Pachfule, H. Wu, Q. Xu and P. Chen, *Nat. Rev. Mater.*, 2016, **1**, 1–17.

201 Z. Huang, S. Wang, R. D. Dewhurst, N. V. Ignat'ev, M. Finze and H. Braunschweig, *Angew. Chem., Int. Ed.*, 2020, **59**, 8800–8816.

202 A. Staubitz, A. P. M. Robertson and I. Manners, *Chem. Rev.*, 2010, **110**, 4079–4124.

203 C. Wang and D. Astruc, *Chem. Soc. Rev.*, 2021, **50**, 3437–3484.

204 M. Yadav and Q. Xu, *Energy Environ. Sci.*, 2012, **5**, 9698.

205 Q. Wang, F. Fu, S. Yang, M. Martinez Moro, M. de los A. Ramirez, S. Moya, L. Salmon, J. Ruiz and D. Astruc, *ACS Catal.*, 2019, **9**, 1110–1119.

206 N. Kang, R. Djeda, Q. Wang, F. Y. Fu, J. Ruiz, J.-L. Pozzo and D. Astruc, *ChemCatChem*, 2019, **11**, 2341–2349.

207 Q. Zhao, N. Kang, M. Martinez Moro, E. Guisasola Cal, S. Moya, E. Coy, L. Salmon, X. Liu and D. Astruc, *ACS Appl. Energy Mater.*, 2022, **5**, 3834–3844.

208 N. Kang, Q. Wang, R. Djeda, W. Wang, F. Fu, M. M. Moro, M. de los A. Ramirez, S. Moya, E. Coy, L. Salmon, J.-L. Pozzo and D. Astruc, *ACS Appl. Mater. Interfaces*, 2022, **12**, 53816–53826.

209 N. Kang, X. Wei, R. Shen, B. J. Li, E. Guisasola Cal, S. Moya, L. Salmon, C. Wang, E. Coy, M. Berlande, J.-L. Pozzo and D. Astruc, *Appl. Catal., B*, 2023, **320**, 121957.

210 K. S. Park, Z. Ni, A. P. Cote, J. Y. Choi, R. D. Huang, R. J. Uribe-Romo, H. K. Chae, M. O'Keeffe and O. M. Yaghi, *Proc. Natl. Acad. Sci. U. S. A.*, 2006, **103**, 10186–10191.

211 S. Zhang, M. Li, L. Li, F. Dushimimana, J. Zhao, S. Wang, J. Han, X. Zhu, X. Liu, Q. Ge and H. Wang, *ACS Catal.*, 2020, **10**, 14903–14915.

212 C. Wang, J. Tuninetti, Z. Wang, C. Zhang, R. Ciganda, L. Salmon, S. Moya, J. Ruiz and D. Astruc, *J. Am. Chem. Soc.*, 2017, **139**, 11610–11615.

213 F. Fu, C. Wang, Q. Wang, A. M. Martinez-Villacorta, A. Escobar, H. Chong, X. Wang, S. Moya, L. Salmon, E. Fouquet, J. Ruiz and D. Astruc, *J. Am. Chem. Soc.*, 2018, **140**, 10034–10042.

214 C. Wang, X. Liu, Y. Wu and D. Astruc, *J. Mater. Chem. A*, 2022, **10**, 17614–17623.

215 N. Kang, R. Shen, B. Li, F. Fu, B. Espuche, S. Moya, L. Salmon, J.-L. Pozzo and D. Astruc, *J. Mater. Chem. A*, 2023, **11**, 5245–5256.

216 C. Wang, Q. Wang, F. Fu and D. Astruc, *Acc. Chem. Res.*, 2020, **10**, 2483–2493.

217 Q. Zhao, X. Liu and D. Astruc, *Eur. J. Inorg. Chem.*, 2023, e202300024.

218 W. Huang, F. Xu, D.-S. Li, D. Astruc and X. Liu, *Carbon Energy*, 2023, **5**, e269.

219 N. Kang, C. Wang and D. Astruc, *Chemistry*, 2023, **5**, 886–899.

220 K. Yamamoto, T. Imaoka, M. Tanabe and T. Kambe, *Chem. Rev.*, 2020, **120**, 1397–1437.

221 L. Liu and A. Corma, *Chem. Rev.*, 2018, **118**, 4981–5079.

222 Y. Chen, S. Ji, C. Chen, Q. Peng, D. Wang and Y. Li, *Joule*, 2018, **2**, 1242–1264.

223 W. J. Wang, J. Ruiz, C. Ornelas and J.-R. Hamon, *ACS Catal.*, 2023, **13**, 1574–1586.

